MARTIN MARIETTA ENERGY SYSTEMS LIBRARIES
3 4456 0064739 8

ORNL/Sub/85-22013/1

ornl

OAK RIDGE NATIONAL LABORATORY

MARTIN MARIETTA

New High Temperature Absorbent For Absorption Heat Pumps

Final Report

W. F. Davidson
D. C. Erickson

OAK RIDGE NATIONAL LABORATORY
CENTRAL RESEARCH LIBRARY
CIRCULATION SECTION
4500N ROOM 175
LIBRARY LOAN COPY
DO NOT TRANSFER TO ANOTHER PERSON
If you wish someone else to see this report, send in name with report and the library will arrange a loan.

Prepared by

ENERGY CONCEPTS COMPANY
627 Ridgely Avenue
Annapolis, Maryland 21401

under
Subcontract 86X-22013V

for

OAK RIDGE NATIONAL LABORATORY
operated by
MARTIN MARIETTA ENERGY SYSTEMS, INC.
for the
U.S. DEPARTMENT OF ENERGY
under Contract DE-AC05-84OR21400

OPERATED BY
MARTIN MARIETTA ENERGY SYSTEMS, INC.
FOR THE UNITED STATES
DEPARTMENT OF ENERGY

Printed in the United States of America. Available from
National Technical Information Service
U.S. Department of Commerce
5285 Port Royal Road, Springfield, Virginia 22161
NTIS price codes—Printed Copy: A04; Microfiche A01

This report was prepared as an account of work sponsored by an agency of the United States Government. Neither the United States Government nor any agency thereof, nor any of their employees, makes any warranty, express or implied, or assumes any legal liability or responsibility for the accuracy, completeness, or usefulness of any information, apparatus, product, or process disclosed, or represents that its use would not infringe privately owned rights. Reference herein to any specific commercial product, process, or service by trade name, trademark, manufacturer, or otherwise, does not necessarily constitute or imply its endorsement, recommendation, or favoring by the United States Government or any agency thereof. The views and opinions of authors expressed herein do not necessarily state or reflect those of the United States Government or any agency thereof.

ORNL/Sub/85-22013/1

NEW HIGH TEMPERATURE ABSORBENT FOR ABSORPTION HEAT PUMPS

FINAL REPORT

W. F. Davidson
D. C. Erickson

Date Published: July 1986

Prepared by

ENERGY CONCEPTS COMPANY
627 Ridgely Avenue
Annapolis, Maryland 21401

under
Subcontract 86X-22013V

for

OAK RIDGE NATIONAL LABORATORY
Oak Ridge, Tennessee 37831
operated by
MARTIN MARIETTA ENERGY SYSTEMS, INC.
for the
U.S. DEPARTMENT OF ENERGY
under Contract DE-AC05-84OR21400

MARTIN MARIETTA ENERGY SYSTEMS LIBRARIES
3 4456 0064739 8

TABLE OF CONTENTS

EXECUTIVE SUMMARY 1

1. INTRODUCTION 2

1.1 Sponsorship 2
1.2 Organization of Report 2
1.3 Background 2
1.4 Prior Work 3

2. SCREENING AND SELECTION OF HIGH TEMPERATURE ABSORBENT 5

3. MEASUREMENT AND ANALYSIS OF HIGH TEMPERATURE ABSORBENT PROPERTIES 9

3.1.1. General 9
3.1.2. Vapor Pressure and Crystallization Temperature 9
3.1.3. Specific Heat 18
3.1.4. Viscosity 21

3.2 Analytically Derived Properties 22

3.2.1. Enthalpy 22
3.2.2. Thermal Conductivity 25
3.2.3. Prandtl Number 27

4. CORROSION AND THERMAL STABILITY 29

4.1 Literature Citations 30
4.2 Experiment 30

5. ANALYSIS OF PERFORMANCE AND ECONOMICS 33

5.1 General 33
5.2 Possible Uses and Cycle Diagrams 33
5.3 Estimation of COP 38
5.4 Calculation of Coefficient of Performance 39

5.4.1. Definitions 39
5.4.2. Example Calculations of COP 36
5.4.3. Comparison with LiBr 42

6. CONCLUSIONS 44

7. RECOMMENDATIONS 45

8. ACKNOWLEDGEMENTS 45

9. REFERENCES 46

APPENDICES

Appendix 1: Chemical Analysis of Industrial Grade Nitrate Salts
Appendix 2: Measured VLE Data
Appendix 3: Calculations for Construction of the Merkel Diagram

FIGURES

Figure 2.1	Screening Results	7
Figure 2.2	High Temperature (260°C) Aqueous Absorbents	8
Figure 3.1	Vacuum VLE Apparatus	10
Figure 3.2	Measured VLE Data	14
Figure 3.3	Atmospheric Boiling Point vs. Concentration	15
Figure 3.4	Solubility Field for High Temperature Absorbent	16
Figure 3.5	Duhring Diagram for High Temperature Absorbent	17
Figure 3.6	Measured Specific Heat of the High Temperature Absorbent	20
Figure 3.7	Viscosity of High Temperature Absorbent	24
Figure 3.8	Merkel Diagram for High Temperature Absorbent	26
Figure 5.1	Derivation of Heat Amplifier Applicability Diagram	34
Figure 5.2	Heat Amplifier Applicability Diagram	36
Figure 5.3	Temperature Amplifier Applicability Diagram	37
Figure 5.4	Heat Amplifier with High Temperature Absorbent	40
Figure 5.5	Temperature Amplifier with High Temperature Absorbent	41
Figure 5.6	COP Comparison Cycle	43

LIST OF TABLES

Table 3.1	Specific Heat Measurements	19
Table 3.2	Viscosity Data Reduction	23
Table 3.3	Prandtl Number Comparison	28
Table 4.1	Aqueous Nitrate Corrosion Tests	32

EXECUTIVE SUMMARY

A new absorption working pair (AWP) for absorption heat pumps has been identified which provides higher temperature capability (260°C), higher lifts, and use of lower cost construction materials, than currently available absorption heat pump working fluid pairs (e.g. $LiBr-H_2O$).

Using water as working fluid, the absorbent is a ternary mixture of $LiNO_3$, KNO_3, and $NaNO_3$ in the preferred proportions of 53, 28, and 19 weight percent respectively. In addition to being thermally stable to well above 260°C, it promotes the formation of a passive and protective corrosion resistant oxide film on both mild steel and all stainless steels.

The thermodynamic, corrosion, and stability properties of this new absorbent have been measured and are reported herein. Additional properties have been analytically derived as necessary to predict the performance capabilities and limitations of an absorption heat pump using the new absorbent.

The ternary nitrate absorbent is useful with waste heat temperatures in the range of 50 to 230°C for providing temperature lifts of up to 58°C for the heat amplifier mode and 90°C for the temperature amplifier mode. This contrasts to the LiBr capabilities of 5 to 150°C waste heat temperatures and 43°C and 51°C respective lifts. In the area where the capabilities overlap, the ternary nitrate has a heat amplifier COP which is about 3 percent larger than that of LiBr in the same cycle, due to the lesser deviation from ideal mixing. For the same reason, the temperature amplifier COP of the new absorbent is a corresponding amount lower than that of LiBr. Thus in the area of overlap, the choice of AWP for a temperature amplifier would involve a tradeoff between the higher COP of LiBr and the lower cost construction materials of the ternary nitrate. For heat amplifier applications in the area of overlap the ternary nitrate is preferred on both counts. For higher temperatures or higher lifts, which are the applications of greatest interest to industry, the ternary nitrate is the only viable choice identified to date.

These results indicate that development should continue. The next step is to build and operate a bench scale pilot plant. This step will provide: (1) the first-ever attainment of 260°C absorption heat pumping, (2) confirmation of thermodynamic and corrosion results in an operational environment, and (3) essential heat and mass transfer data. These results are needed to establish an acceptable level of confidence for private sector commercialization and large scale industrial use.

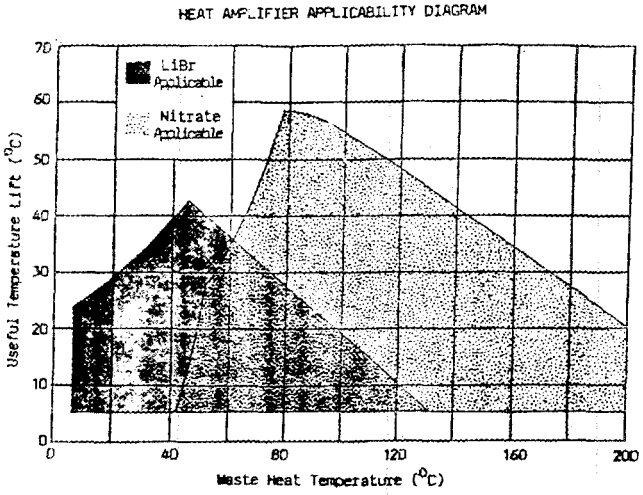

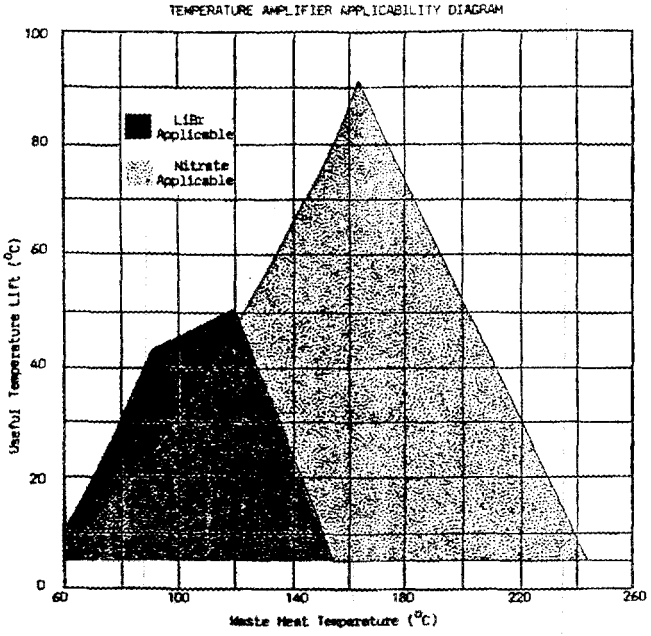

1. INTRODUCTION

1.1 SPONSORSHIP

This report is an account of research performed by Energy Concepts Company for the Oak Ridge National Laboratory pursuant to Martin Marietta purchase order 86X22013. The ORNL Project Manager is Mr. Stephen I. Kaplan.

The objectives of Phase I of the research are to screen and select an absorption working pair capable of operation up to 260°C, at high lifts, and with low cost metallurgy (preferably mild steel); to measure and analyze the thermodynamic, corrosion, and stability properties; and to calculate the predicted performance of an absorption heat pump incorporating this absorbent.

Phase II, if implemented, will involve construction and operation of a proof-of-concept test unit. This will permit measurement of key mass transport properties in addition to demonstrating operational achievement of the research objectives.

1.2 ORGANIZATION OF REPORT

In this report, the screening results and the rationale for the selected absorbent composition are presented in section 2. The experimentally measured properties and analytically derived properties of the selected absorbent are in section 3. Section 4 presents the corrosion and thermal stability data. The cycle performance calculations, including example applications and a comparison to LiBr, are in section 5. The conclusion, presented in section 6, is that this absorption working pair does indeed provide the long sought characteristics, and therefore a continuation into phase II is recommended.

1.3 BACKGROUND

Large industrial and commercial scale absorption chillers came into widespread use about 35 years ago. In the last ten years, that same technology has been extended to heat pumping applications (all temperatures above ambient). However, the sphere of application of absorption heat pumping has remained extremely limited due to the temperature limitations of existing absorption working fluid pairs.

At any industrial or commercial plant site, there are usually at most two or three appropriate points at which heat pumping should be applied. Those points may be identified by "pinch" or "target" analysis (Duran, 1986). The temperature at that point, and the amount of temperature lift required to do heat pumping at that point, will vary widely from plant to plant and process to process. Thus a need exists for industrial scale heat pumps capable of operating at many different temperature levels and temperature lifts.

The above need has long been recognized by researchers in the absorption cycle field. The generally recognized limitations of the currently used LiBr-H_2O absorption working pair are:

1) Maximum lift of 45°C, as determined jointly by limited solubility field and by corrosion (Erickson, 1985).

2) Maximum absorbent temperature of 170°C, based on corrosion rate of Cu-Ni or ferritic stainless steel.

3) No use of austenitic stainless steel due to halide stress corrosion susceptibility.

In 1982, at a conference convened to review the state-of-the-art of absorption working pairs, the continuing need for higher lifts and temperatures than those possible with LiBr-H_2O was emphatically reiterated (Raldow, 1982).

When dealing with absorption cycles which will pump heat from near or above ambient temperature, as opposed to refrigeration and air conditioning cycles, water has overpowering advantages as choice of working fluid. It has exceptionally high heat of evaporation, exceptionally high film heat transfer coefficient, very low viscosity, exceptionally low cost, and is safe, nontoxic, and nonflammable. Its only minor detractions are low pressure, high heat capacity, and potential corrosivity. Thus the real choice in the search for high temperature absorption working pairs reduces to selection of a suitable aqueous absorbent. The problem is to find an aqueous absorbent that allows full realization of the major advantages inherent to selection of water as working fluid, i.e., one which does not concurrently introduce too many or too severe offsetting disadvantages.

1.4 PRIOR WORK

Energy Concepts Company first identified the alkali nitrates and nitrites as good candidates for absorbing water at high temperature in 1981. These salts have been used by Energy Concepts in anhydrous form in a high temperature chemical air separation research project since 1977 (Erickson, 1983). Experience with water contamination of these salts, plus knowledge of related industrial experience with them, indicated that they were highly stable and non-corrosive at high temperatures, and that mixtures had low melting points and good water absorbing properties. After some preliminary experimentation, a research proposal was submitted to the Department of Energy in 1982, and also a U.S. patent application was filed.

Energy Concepts has continued independent research on this absorbent since that time until June 1985 when the current contract began. This research consisted of measuring the atmospheric pressure boiling temperature of various mixtures as a function of concentration, the crystallization

temperatures, and, for the most promising combinations, the high temperature corrosion and stability. In addition to testing many combinations of alkali metal nitrates, various other additives were also tested, including nitrites, hydroxides, and halides. One major finding of this prior work was that no clear net benefit was gained from including any of the other additives. This provided an important starting place for the contracted effort, focusing it exclusively on the alkali metal nitrate combinations.

Two U.S. patents have now been issued to Energy Concepts on this technology: U.S. Patent 4454724, which discloses mixtures including both nitrates and nitrites; and U.S. patent 4563295, which discloses the ternary alkali metal nitrate absorbent. One additional U.S. application is still pending.

2. SCREENING AND SELECTION OF HIGH TEMPERATURE ABSORBENT

The water dissolving characteristics of the various pure alkali metal nitrates and several discrete nitrate mixtures are available in the literature. Both pure $LiNO_3$ and equimolar $LiNO_3$-KNO_3 were measured at ORNL (Braunstein, 1971), and $NaNO_3$, KNO_3, and several other binary compositions are tabulated by White and by Combes (Inman, 1981).

Analysis of the literature data reveals that none of the pure nitrates have an acceptable solubility field for an absorption cycle, nor do the $NaNO_3$-KNO_3 combinations. Some of the $LiNO_3$-KNO_3 or $LiNO_3$-$NaNO_3$ combinations have an acceptable high temperature solubility field, but their solubility at low temperatures is extremely limited.

Water solutions of $LiNO_3$ exhibit a substantial negative deviation from Raoultian behavior, although not as much as LiBr. $NaNO_3$ solutions exhibit approximately ideal behavior, and KNO_3 has a positive deviation.

The heat of mixing has two direct effects on absorption cycles. First, it affects COP by setting the approximate heat duty ratio of generator/condenser and absorber/evaporator. For ideal mixing, those ratios are close to unity, and they increase proportional to the degree of negative deviation. Thus high negative deviation absorbents will have lower heat amplifier COPs and higher temperature amplifier COPs than ideal absorbents. Secondly, more negative deviation results in lower solution concentrations at a given boiling point elevation. The practical result is more solution pumping power required for the more nearly ideal absorbents. When using water as working fluid, which characteristically requires only low solution circulation rates due to the high latent heat of evaporation, the pumping power only becomes a problem with actual positive deviation mixing, for example when glycols are used as absorbent.

The implications of the above generalities on the screening and selection process are that compositions with as much $LiNO_3$ as possible should be selected, owing to the negative deviation and low molecular weight, and that sufficient $NaNO_3$ and KNO_3 should be added to extend the solubility field (crystallization temperatures) the required amount, and that the $NaNO_3$ and KNO_3 proportions should be selected to minimize the total amount added.

To implement this process over two thousand data points were measured of the atmospheric pressure boiling temperature and crystallization temperature of various absorbent compositions and concentrations. The composition refers to the anhydrous makeup of the absorbent, and the concentration refers to the amount of water present. In order to help assimilate this data, several triangular three-axis graphs were prepared, with the weight percent $LiNO_3$ on one axis, the weight percent H_2O on the second, and the weight percent "all other" on the third axis. The graphs were distinguished by

the identity of "all other": on three graphs, it was $NaNO_3$ and KNO_3 in weight ratios of 2:1, 1:1, and 1:2 respectively, and others included additional nitrates. Figure 2.1 is the most representative example of these graphs, reflecting the 1:1 ratio.

These graphs revealed that the highest boiling temperatures for a given water concentration were obtained when KNO_3 and $NaNO_3$ were present at ratios between 1:1 and 2:1. Although little variation in boiling temperature was noted over that range, the KNO_3 rich compositions did have markedly lower crystallization temperatures. It was concluded that somewhat more KNO_3 than $NaNO_3$ would be best.

Next, it was necessary to select target values of lift and evaporator temperature, to determine how low a crystallization temperature was required, i.e., how much total KNO_3 and $NaNO_3$ was required. (Figure 2.2 illustrates the selection rationale.) Recognizing that most industrial waste heat is available at temperatures above 75°C, and that LiBr can handle those instances of lower waste heat temperature, an evaporator temperature of 75°C was postulated. This set the absorber pressure. For this evaporator temperature, it was postulated further that the solubility field should allow a temperature difference between absorber and evaporator of 75°C ΔT. This set the absorber temperature at 150°C, point A. Finally, a 15°C absorber margin from crystallization established point B. This point thus should coincide with the onset of crystallization. Several additional tests in the region of composition of interest led to the final selection of 53 w/o (weight percent) $LiNO_3$, 28 w/o KNO_3, 19 w/o $NaNO_3$.

The full onset of crystallization boundary for this composition is shown in Figure 2.2. Note that for any system pressure above that corresponding to a 68°C evaporator, higher lifts and higher solution concentrations cannot result in crystallization. This is because the crystallization curve for the ternary nitrate bends downward with increasing temperature--the water vapor pressure must reach zero at the anhydrous melting point of 193°C.

Figure 2.2 was prepared from screening data using the assumption that all compositions tested had approximately equal slopes on the RTlnP vs. T plot. The crystallization lines illustrate the effect on the solubility field of varying the nitrate composition. By varying the composition of the salt, several ternary nitrate mixtures were created, some allowing evaporator temperatures as low as 60°C. Quaternary mixtures incorporating $CsNO_3$ can further decrease the evaporator temperature to 45°C. However, those mixtures have lower lifts and require more pumping power than the selected mixture, due to their lower $LiNO_3$ content. For general purpose industrial use, the selected composition is believed to be most applicable and appropriate, and hence that composition is the focus of the remainder of the report.

The new absorbent has a wider solubility field than any of

FIGURE 2.1 SCREENING RESULTS

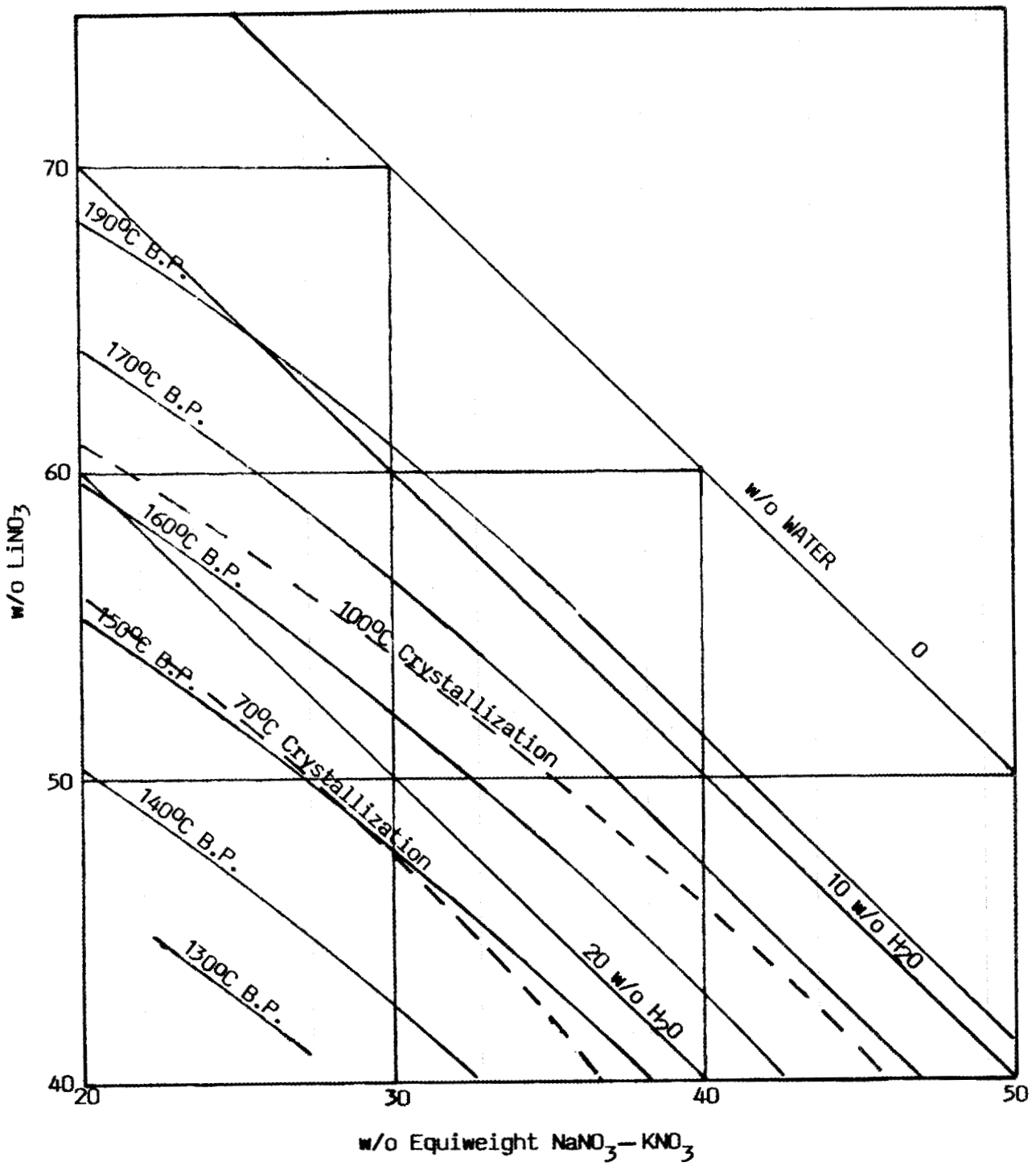

FIGURE 2.2

HIGH TEMPERATURE (260°C) AQUEOUS ABSORBENTS

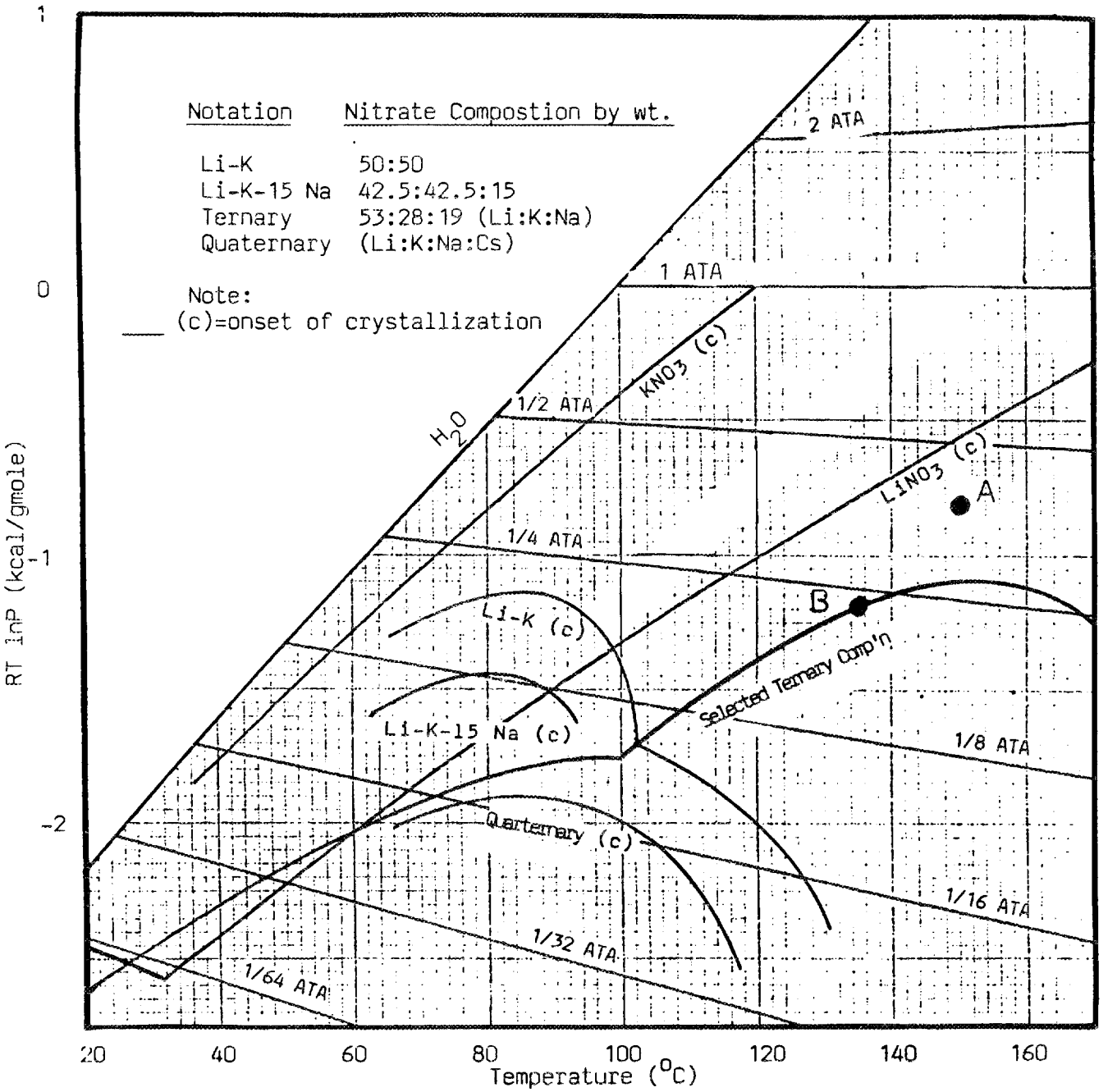

the nitrates pictured except the quaternary mix. It also has a very favorable shutdown characteristic requiring dilution to only 42 w/o H_2O to remain liquid at 20°C. In contrast pure $LiNO_3$ must be diluted to 59 w/o H_2O at 20°C. The costs of $LiNO_3$, KNO_3, and $NaNO_3$ respectively are \$2.75, \$0.40, and \$0.20 per pound. The cost of the ternary nitrate is one-third the cost of LiBr.

3. MEASUREMENT AND ANALYSIS OF HIGH-TEMPERATURE ABSORBENT PROPERTIES

3.1.1. General

The thermodynamic properties of an absorbent which have greatest impact on the thermodynamic performance of an absorption cycle are the vapor pressure, the crystallization temperature, the specific heat, and the viscosity, all as a function of temperature and solution concentration. Much of this data is available on the individual alkali nitrates in the literature, but little or none is available on aqueous mixtures. Furthermore the individual salts crystallize at much lower concentrations than do mixtures, so no data was available at the concentrations of interest and it was therefore necessary to measure the above parameters in laboratory experiments.

3.1.2. Vapor Pressure and Crystallization Temperature

3.1.2.1. Purpose

For an absorption cycle, pressure-temperature-concentration (P-T-X) data are fundamental for cycle analysis. The vapor-liquid-solid equilibrium pressure diagram of the working fluid with its absorbent reveals what cycles are feasible. In addition these data are useful to derive enthalpies of solution. Therefore, the objective of these experiments was to obtain the vapor pressure and crystallization temperature of the equilibrium liquid absorbent over a range of concentrations and temperatures, and with an accuracy sufficient for deriving the enthalpy of solution.

3.1.2.2. Method

Both subatmospheric and superatmospheric pressures were measured. Glass apparatus was used for tests in the vacuum region so that liquid levels, boiling, and crystallization could be seen. A stainless steel pressure vessel was used for the high pressure vapor liquid equilibrium (VLE) measurements.

The apparatus used for measurements in the vacuum region is pictured in Figure 3.1. The apparatus and procedure are described as follows. The solution sample to be tested (typically 100 cm^3) was placed in a 250 cc glass flask and the flask was then evacuated. The temperature of the solution was

FIGURE 3.1 VACUUM VLE APPARATUS

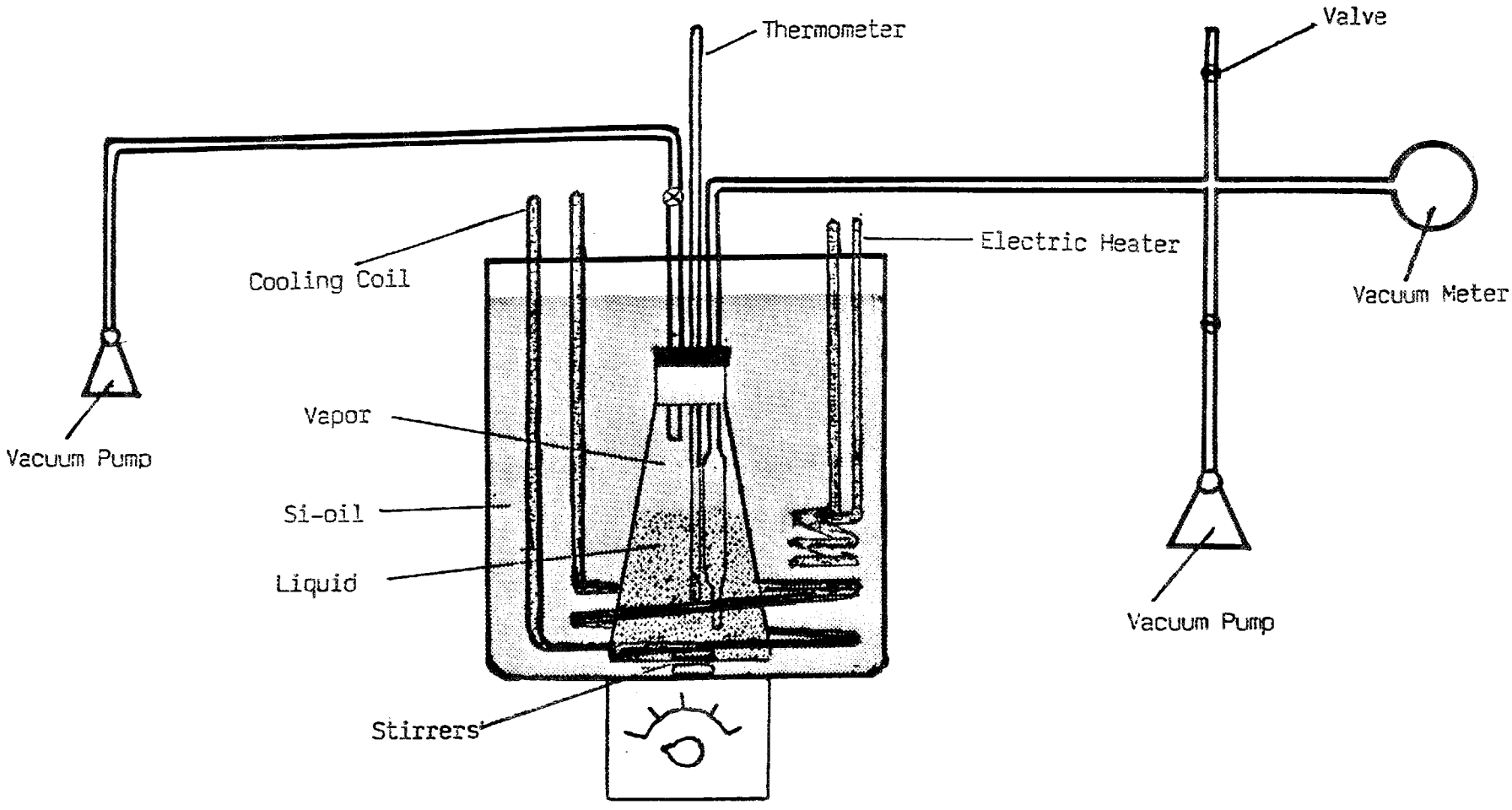

controlled by immersing the entire flask in a silicon oil circulating bath. The temperature of the bath was controlled to within 0.01K. The bath and the sample was stirred continuously by a magnetic stirrer. The temperature of the sample was measured with a mercury-glass thermometer, with the bulb in the liquid phase of the sample. The pressure was determined by a Heise vacuum gage connected to a reference pressure system operating with air. The accuracy of this gage is 0.2% of full scale (760 mm Hg). The reference pressure was adjusted to cause the liquid column of the sample inside a tube located in the sample flask to be the same height as the liquid level of the surrounding sample. In this way pressure equilibrium was maintained.

The composition of the sample was determined by weighing directly into the flask the required amounts of salt and water. The accuracy of the balance was 0.1 g. The total weight of each sample was over 100 grams. The water content of the salt as delivered by the manufacturer was checked periodically by drying a sample and reweighing.

In order to minimize air leakage, the flask, stopper and tubing were sealed with silicon rubber. Any air inside the flask and solution was removed as follows. The solution was heated to its boiling point for five minutes and after cooling was evacuated for ten minutes by a vacuum pump, while the sample was stirred. The temperature was always kept above the crystallization temperature. Finally, the water loss due to evaporation during the process was confirmed by weighing. For solutions of the three highest concentrations, the sample was weighed, dried, and re-weighed after each VLE run.

In order to ensure that no air which might have leaked into the flask affected the pressure readings, the sample container was evacuated for a few seconds once or twice during the course of the measurements for each composition. Determination of the sample weight at the conclusion of the experiment indicated no measurable concentration change as a result of the periodic use of the vacuum pump.

The apparatus and procedure were verified against the vapor pressure curves of both water and a LiBr solution.

The high pressure apparatus consists of a four inch diameter by 24 inch long stainless steel vessel which is electrically heated by two strip heaters, is instrumented for temperature and pressure, and is insulated. Saturated solution temperature is monitored by a type-K thermocouple located about 1.5 inches below the liquid surface within an axially-mounted well. The same thermocouple activates the temperature controller. A separate thermocouple measures wall temperature. The solution charge, approximately four liters, fills the vessel to the height of the strip heaters. The upper vessel surface and pressure instruments are not insulated so as to provide condensing surfaces for reflux of the water vapor. The reactor vessel has a full diameter opening at the top which is sealed by an O-ring seal.

Pressure instruments and vents are located on the cap.

Before operation the apparatus was evacuated to 3 mm Hg absolute pressure for bulk removal of noncondensables. Once heated to above atmospheric pressure, further noncondensables were removed via an overhead collection tube and vent port. For pressures from vacuum to 100 psig, a Bourdon tube pressure gage with a 6" dial was used. For pressures above 100 psig, a Bourdon tube pressure gage with 0 to 400 psig scale (4 inch dial) was used. Both gages have accuracies of 2%-1%-2% (full scale).

Solution composition and concentrations were determined by weight. For superatmospheric pressure VLE, technical grade industrial salts were used. Purity and composition of these salts is detailed in Appendix 1. Wetness of the individual stock salts was determined by drying. Three concentrations were tested. The concentration of the solution in this apparatus was increased between runs in the following manner. The apparatus includes an uninsulated 1" diameter by 40 inch long tube connected via isolation valves to the solution vessel cap. When the isolation valves were opened, steam migrated to and condensed in this condenser tube. The approximate amount collected was sensed with temperature-sensitive indicator crayons. The condenser tube, having been previously weighed, was then removed and weighed to accurately determine the amount of water removed.

For each solution concentration, vapor pressure was recorded at solution temperatures above atmospheric boiling point in increments of approximately 5 degrees C for at least 12 readings. Vacuum conditions were avoided to insure that no air could enter the vessel through leaks. Minor steam leaks were detected when pressure was over 60 psig. Measurements were taken when equilibrium conditions were achieved, i.e., when the temperature controller indicated that the new temperature set point had been reached and ten minutes had passed without temperature change.

After the final run, samples of solution were removed, dried, and weighed for accurate determination of concentration.

If hysteresis were present (difference between pressure readings during temperature increase and decrease) it would be most detectable at the highest concentration tested. For this concentration (89%) data was collected for incremented and decremented temperatures. No hysteresis was indicated.

To test for effects of stratification within the absorbent solution the solution was vigorously shaken for 60 seconds and another data set was taken. No significant difference was observed.

Crystallization temperatures were obtained by incrementally adding distilled water to a molten solution of known starting composition, cooling slowly while stirring, and

noting the temperature where cloudiness or precipitate first appeared. Usually at least 5 to 10°C additional cooling was possible before extensive slushiness was present. The crystallization temperatures were double-checked by incrementally increasing the concentration by boiling, and cooling the solution to crystllization from several boiling temperatures. The nitrate system never exhibited the subcooling which is frequently encountered with aqueous LiBr or alkali hydroxide systems.

3.1.2.3. Results

The measured data collected from both the vacuum and high pressure tests are plotted in Figure 3.2. The data are also tabulated in Appendix 2.

The coordinates used in Figure 3.2, RTlnP vs T, are very useful for plotting VLE data of binary solutions. It is analogous to the Ellingham diagram, which is routinely used for plotting chemical reaction equilibria. The temperature scale is linear, and most substances plot very nearly as straight lines. Also, this diagram is not dependent upon any reference substance; different fluids may be plotted on the same diagram. The pressures are read directly from a logarithmic scale.

For any given concentration, the slopes of the plotted RTlnP vs T temperature data matched closely when comparing the high and low pressure data sets. However, cross-plotting of concentration data against temperature revealed inconsistencies in the measured concentrations. Figure 3.3 is a plot of atmospheric pressure boiling temperature vs. concentration for both vacuum and high pressure runs taken from P-T lines plotted Figure 3.2. The curve fit through these data was strongly weighted to the four highest concentration data points as these were obtained by drying the sample after testing. These points as well as the lower concentration data at 50, 60, 70 w/o (weight percent) fall on a smooth curve. This curve was used to reassign concentrations for those solutions which did not fall directly on the curve. It is believed that those points not falling on this curve are due to difficulties in drying the salts during the early work.

Figure 3.4 is the resulting P-T-X diagram. It was constructed by preserving the slope of the P-T lines from the measured data, and by taking concentrations from the curve in Figure 3.3. The crystallization temperatures are also plotted on this diagram, thus defining the solubility field of the high temperature absorbent.

The Duhring diagram is another format for presenting P-T-X data. It plots absorbent temperature against working fluid temperature for the same pressure. This is the historical format for presenting P-T-X data for absorption refrigeration cycles. It has the advantage for the high temperature AWP, as it does for LiBr, that constant

FIGURE 3.2

MEASURED VLE DATA

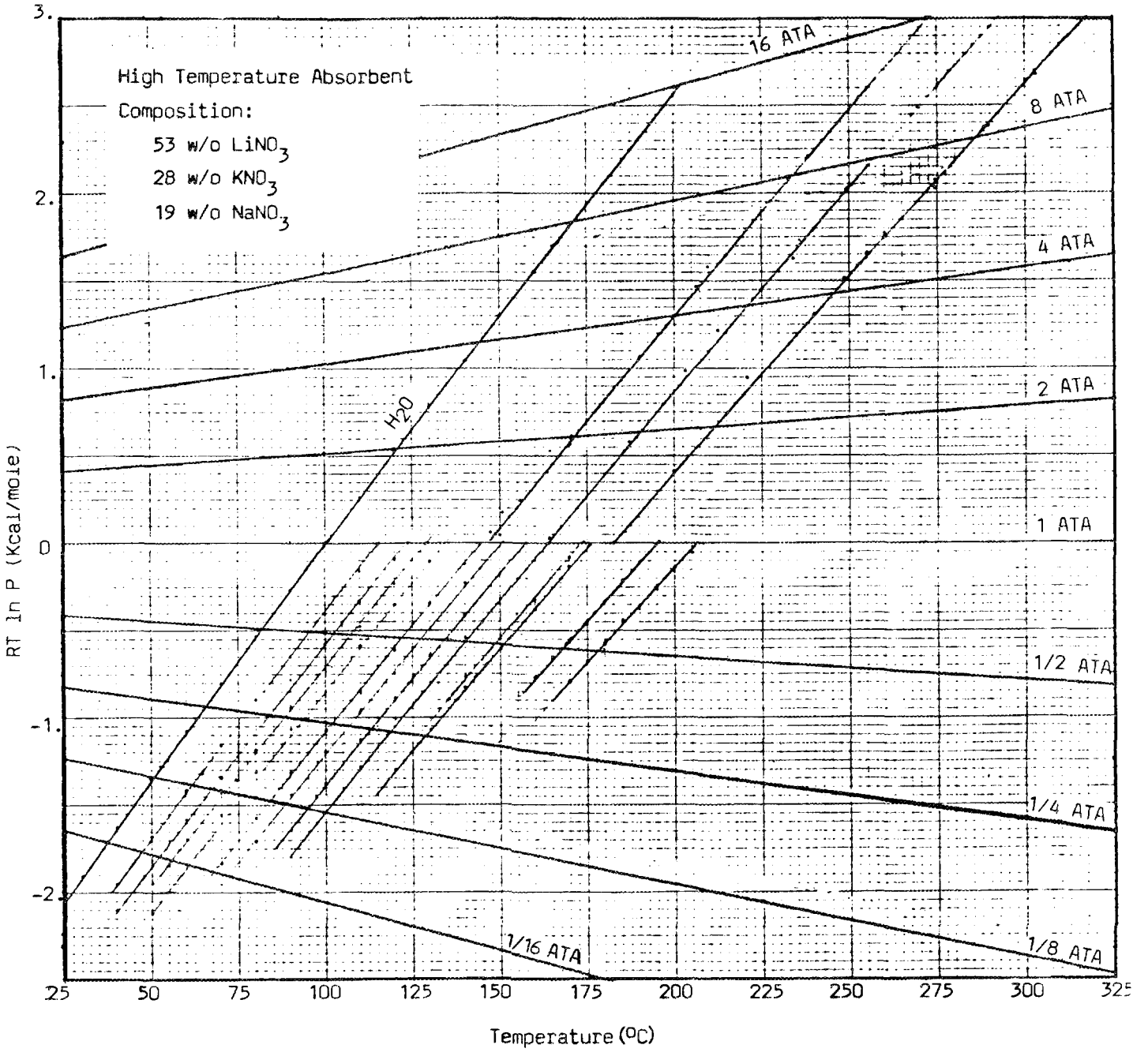

FIGURE 3.3

ATMOSPHERIC BOILING POINT VS. CONCENTRATION

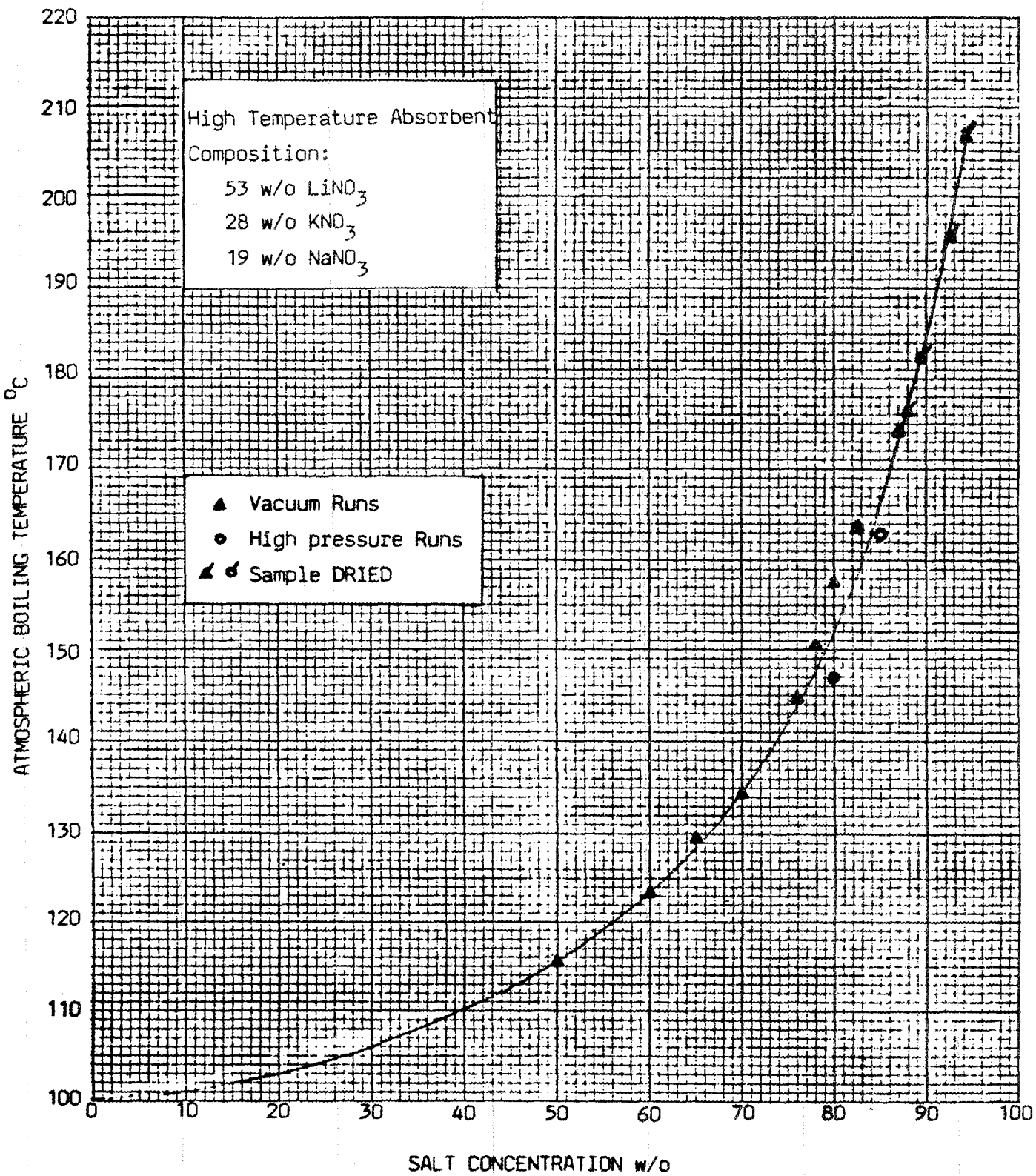

FIGURE 3.4

SOLUBILITY FIELD FOR
HIGH TEMPERATURE ABSORBENT

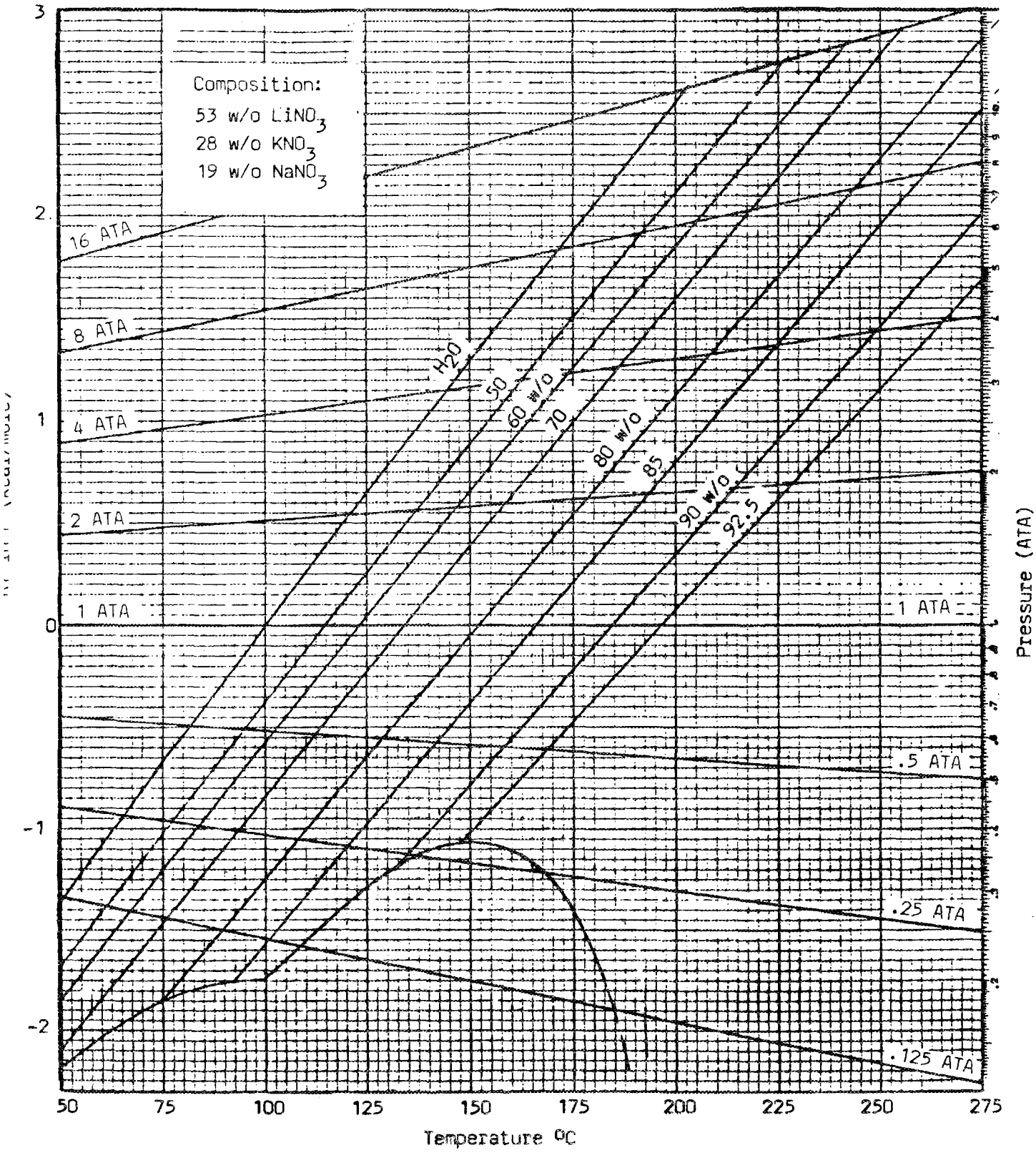

FIGURE 3.5

DUHRING DIAGRAM FOR
HIGH TEMPERATURE ABSORBENT

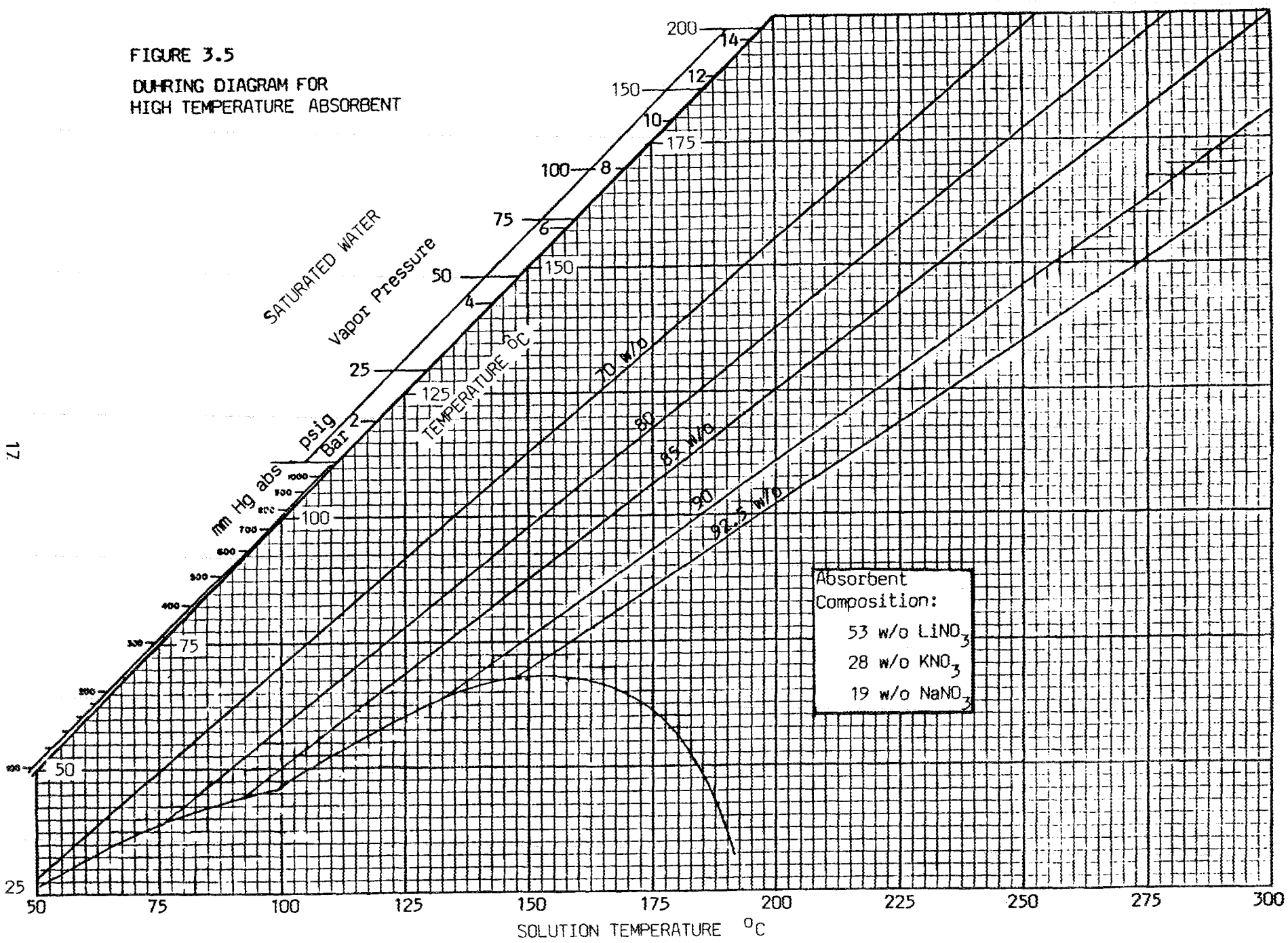

concentration lines are quite linear at low concentrations. Thus the slopes of these lines can be read with confidence. The enthalpy analysis below takes advangtage of this. Figure 3.5 is the Duhring diagram for the high temperature AWP. A disadvantage is that because this scale artificially linearizes water, pressures can be read only in reference to the saturation temperature of water.

3.1.3. Specific Heat

3.1.3.1. Purpose

The specific heat required and measured in this work is the change in enthalpy with temperature at constant pressure. This property is used in deriving solution enthalpies, and in estimating heat transfer properties.

3.1.3.2. Method

Specific heats are measured by calorimetry. The apparatus and technique used for these measurements was similar to that used by Dewing in measuring heat capacities of liquid anhydrous sodium and potassium nitrates except that the calorimeter walls were adiabatic instead of isothermal. (Dewing, 1975). In addition, a literature search and estimation technique were used to generate an estimated value for comparison to the measured results.

For the laboratory measurements, solutions of desired concentration were prepared by weighing. The solution was heated to just above the desired starting temperature, then poured into a thermos bottle and allowed to equilibrate. A copper block, used as the reference substance, was cooled to 0°C in an ice bath. The copper block was immersed in the solution in the thermos bottle and the thermos was capped with a styrofoam lid with a penetrating thermometer. The thermometer was a calibrated mercury thermometer, readable to 0.1°C. The specific heat of the copper block was determined in an identical manner using distilled water as the reference substance.

Heat loss from this apparatus to the environment presented a systematic error. This was accounted for by observing the temperature drop with time of the solution in the thermos without adding the copper, and correcting the ending temperatures accordingly.

All experiments were performed at atmospheric pressure. Therefore, measurements could be made only for temperatures between solidification and atmospheric boiling temperatures for each concentration.

3.1.3.3. Results

Table 3.1 lists the experimental data, and Figure 3.6 displays the results for specific heat of the high temperature absorbent. The greatest number of measurements were taken for the 80 w/o concentration. The specific heat for this

TABLE 3.1

SPECIFIC HEAT MEASUREMENTS

Concentration w/o	Temperatures (C) Starting	Ending	Specific Heat (kJ/kg K)
80	103.5	97.2	2.430
	134	124.5	2.118
	154	143.2	2.045
80	101	94.8	2.494
	130.3	121.3	2.221
	153	142.4	2.158
90	150	140.2	2.264
	179	165.8	2.071
90	150	138.7	2.265
	180	162.9	2.051
80	110	102.4	2.4509
	130	120.7	2.343
	140	129.9	2.2427
	145	134.1	2.213
80	110	102.4	2.381
	130	120.9	2.310
	145	134.5	2.2128
90	150	138.9	2.177
	180	165.7	2.036

Copper block reference substance:

mass = 215.3 (g)
Specific heat = 0.3867 (kJ/kg K)

High Temperature Absorbent

Composition:

53 w/o $LiNO_3$

28 w/o KNO_3

19 w/o $NaNO_3$

FIGURE 3.6

MEASURED SPECIFIC HEAT OF THE

HIGH TEMPERATURE ABSORBENT

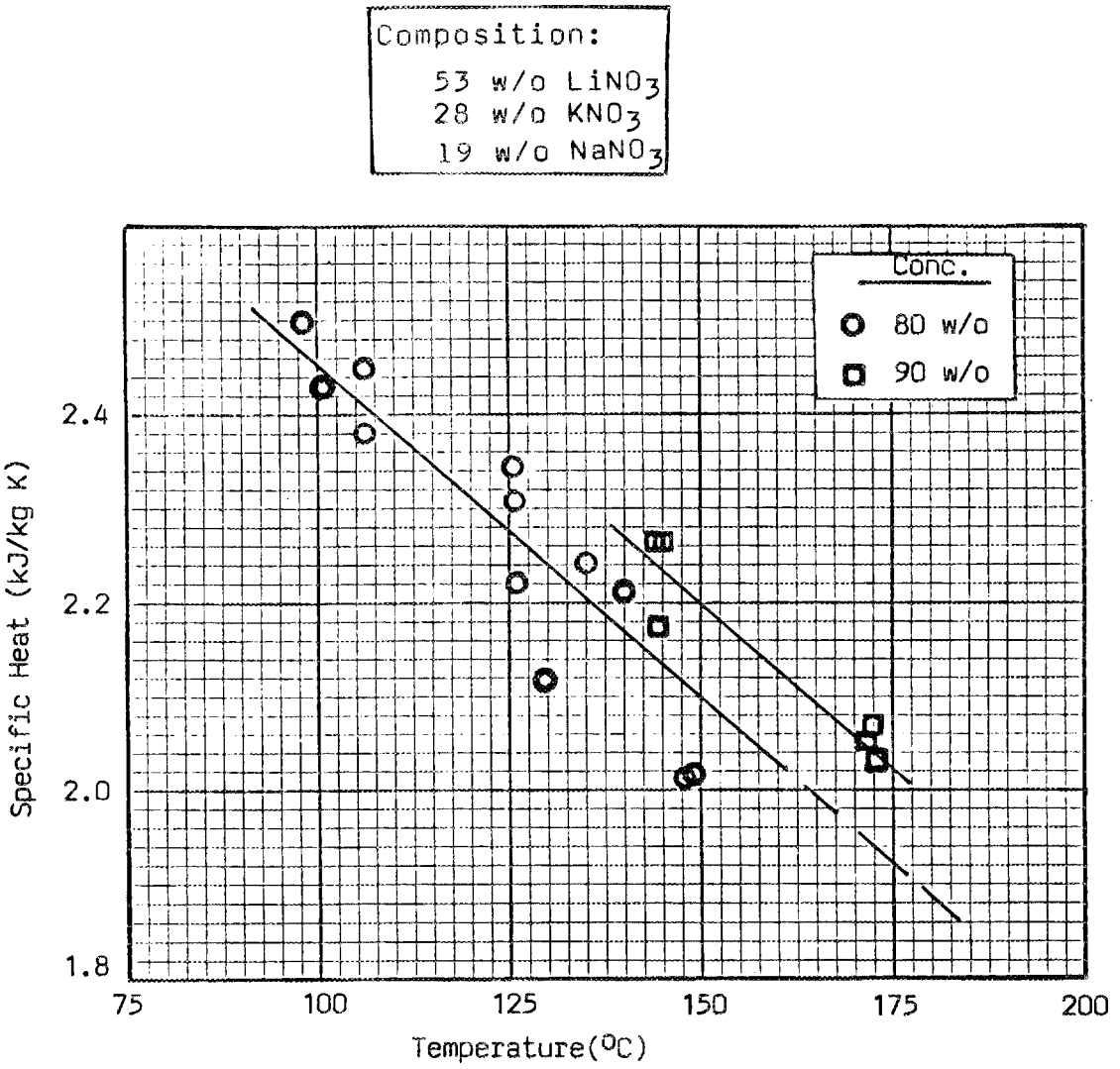

the 80 w/o concentration. The specific heat for this concentration was used to construct the enthaply chart in section 3.2.2. The regression line through the data for 80 w/o gives the following relationship:

$$\text{Specific Heat (kJ/kgK)} = 3.164 - 0.007707 \times T(C)$$

for: 80 w/o salt, between 90°C and 150°C

In the literature search, references were obtained which individually address each of the three nitrate species in aqueous solution over a range of concentrations and temperatures (Puchkov, 1973; Winkelman, 1873; Parker, 1965; Hougen, 1943). Unfortunately, the temperatures and concentrations covered do not overlap in the desired range.

The anhydrous specific heats are sufficiently identified in the literature to permit their use in estimating combined specific heats for the temperature range of interest. In particular, equations for specific heat as a function of temperature are available for all three nitrates (Ichikawa, 1983; Marchidan, 1968; and Barin, 1973).

There is presently no theoretical basis for combining specific heats of individual species. It is customarily done on a mole fraction basis. However, that method of combining values ignores the temperature effects of heats of mixing (Reid, 1977). With this caveat in mind, the above mentioned functions were combined with tabulated NBS date (Haar, 1984) for specific heat of saturated liquid water by mole-fraction averaging for the 80 w/o solution. This tabulation suggests that specific heat values of 1.8 kJ/kgK to 2.2 kJ/kgK should be expected, which are in the range of the experimental results. However, it indicates that specific heat increases with temperature for these conditions, while the experimental results evidence decreasing specific heat with temperature.

Published data indicate that such a reversed temperature relation is not the general rule, but that it does occur, such as in the case for pure $NaNO_3$ in aqueous solution between 19 and 24 w/o and between 275 and 340°C (Puchkov, 1973). Also, 70 w/o LiBr exhibits a loss of approximately .03 kJ/kgK for each K greater than 130°C, at least up to 180°C (McNeely, 1979). With Reid's caveat in mind, the mole-averaged, literature-based estimate for the four-component mixture can not be considered reliable. It is presented merely as a confirmation of the general magnitude of the experimentally derived results.

3.1.4. Viscosity

3.1.4.1 Purpose

Viscosity is the measure of a fluid's internal friction. It influences the amount of parasitic pump work required to maintain flow. More importantly, it influences heat transfer film coefficients and thus overall heat transfer and surface

area requirements for heat exchangers. Absorption heat pumps (AHPs) are comprised essentially of heat exchangers. The simplest closed cycle continuous AHP has five heat exchangers, each involving two fluids and two surface film coefficients. Six of the ten surfaces exchange heat with AWP fluids--two with pure water or steam, and four with the high temperature absorbent. The viscosity measurements are used to calculate Prandtl number, which is one determinant of those surface film coefficients.

3.1.4.2. Method

A Cannon-Fenske viscometer of size 100 (3 to 15 cSt) was used in accordance with ASTM Method 445 to measure kinematic viscosity. The viscometer was calibrated in accordance with ASTM Method 446 with S-6 calibration oil. Corresponding densities were measured by recording weight and volume in a 100 ml graduated cylinder immersed in the same temperature control bath. Dynamic viscosity is the product of kinemetic viscosity multiplied by density. Measurements were taken for four concentrations at temperatures ranging from just above liquidus to below atmospheric boiling point.

3.1.4.3. Results

Table 3.2 presents the data and calculation of dynamic viscosity of the high temperature absorbent. Extrapolation beyond the atmospheric boiling points is considered acceptable as these data closely follow the generally accepted Andrale relation for viscosity variance with temperature (Reid, 1977). Figure 3.7 presents the results graphically, including extrapolation to 260°C.

3.2 ANALYTICALLY DERIVED PROPERTIES

3.2.2. Enthalpy

3.2.1.1. Purpose

Knowledge of saturated solution specific enthalpy facilitates energy balance calculations for cycle analyses.

3.2.1.2. Method

Specific enthalpy is not easily measured directly; it is usually derived analytically from other measured properties. The method used herein is that developed by Haltenberger (1959) and employed by McNeely (1979) for evaluating enthalpy of aqueous LiBr solutions. It applies where the absorbent exhibits good linearity on the Duhring plot, as is the case with this high temperature absorbent. It relies heavily on steam table data, and requires specific heat data at only a single solution concentration.

A full discussion of this method is contained in both of

TABLE 3.2

VISCOSITY DATA REDUCTION

High Temperature Absorbent

Composition:

53 w/o $LiNO_3$

28 w/o KNO_3

19 w/o $NaNO_3$

Concentration (w/o)	Temperature (°C)	Period (sec)	Kinemetic Viscosity (cSt)	Density (g/cm^3)	Dynamic Viscosity (cP)
80	138.8	163	2.335	1.641	3.8317
80	126.2	190.9	2.735	1.648	4.507
85	139.7	209.1	2.996	1.711	5.126
85	122.7	268.7	3.850	1.720	6.622
85	101.0	397.7	5.698	1.730	9.858
90	165.3	217.6	3.118	1.757	5.489
90	154.8	250.3	3.586	1.763	6.322
90	144.5	294.3	4.216	1.7695	7.460
78	143.2	139.1	1.993	3.205	2.335
78	99.5	252.8	3.622	1.6465	5.964
78	121.2	186.9	2.678	1.632	4.370
58	107.4	74.45	1.067	1.415	1.510
58	116.5	68.5	0.981	1.406	1.379

Viscometer constant = .014327 (cSt/sec.)

FIGURE 3.7

VISCOSITY OF HIGH TEMPERATURE ABSORBENT

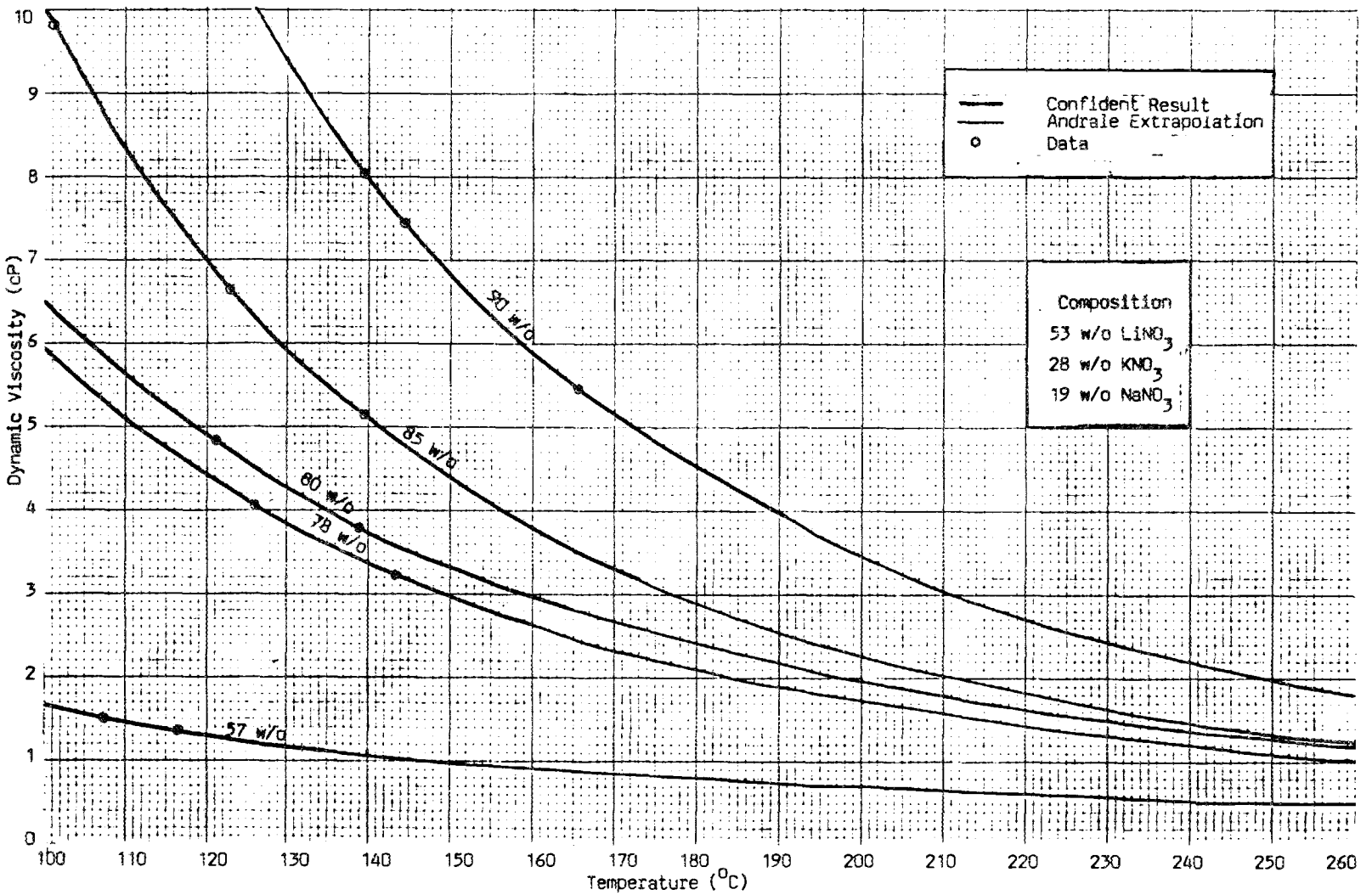

the above references. The calculations and intermediate results are presented in Appendix 3. Briefly, the method uses the slopes of the constant concentration lines in the Duhring diagram. This slope is the ratio of two Clapeyron equations--one for the solvent and one for the solute, both at the same pressure. The only unknown in the resulting single equation is the latent heat of evaporation of the saturated solution. Subtracting this from the enthalpy of the superheated steam leaves the saturated liquid enthalpy of the solution. Haltenberger's approach is to analytically add and subtract water at constant temperature from a base concentration to generate enthalpy isotherms for varying concentrations. This is repeated for various temperatures using specific heat for a base concentration only.

3.2.1.3. Results

Figure 3.8 is the resulting enthalpy-concentration-temperature (H-X-T) diagram for the high temperature AWP. This plot is known as a Merkel diagram. It is used below to calculate cycle energy balances and COP. The reference state for Figure 3.8 is $0^{o}C$, so it can be used directly with standard steam tables.

3.2.2.3. <u>Thermal Conductivity</u>

3.2.2.1. Purpose

Thermal conductivity strongly influences the heat transfer through the convective films which form at heat transfer surfaces. Accurate knowledge of this property is necessary for designing actual units, but contributes little in assessing cycle performance. Because of this and because direct measurement is expensive, it was not an objective of this study to measure, but it was an objective of this study to estimate thermal conductivity of the high temperature absorbent.

3.2.2.2. Method

A literature search and an estimation technique were used to estimate thermal conductivity. Values have been reported in the literature for aqueous $NaNO_3$ and KNO_3--two of the ternary components--and also for several related salts. Most data was for $20^{o}C$, but temperature dependence was shown to be very slight and also could be estimated. Thus literature data presented a basis for an estimate for the conductivity of the ternary nitrate.

Literature values for soultions of pure $NaNO_3$ and pure KNO_3 were available for concentrations less than 40 w/o (Lundolt, 1968 and Vargaftik, 1975). These were linearly extrapolated to higher concentrations assuming marked decrease in conductivity with increasing concentration. From 40 w/o to 80 w/o $NaNO_3$ was reduced by 13 percent, and KNO_3 by 26 percent. No thermal conductivity data were available for $LiNO_3$. However, the bromide salt for each of the cations were reported in Landolt

FIGURE 3.8

MERKEL DIAGRAM

SPECIFIC ENTHALPY OF THE HIGH TEMPERATURE ABSORBENT

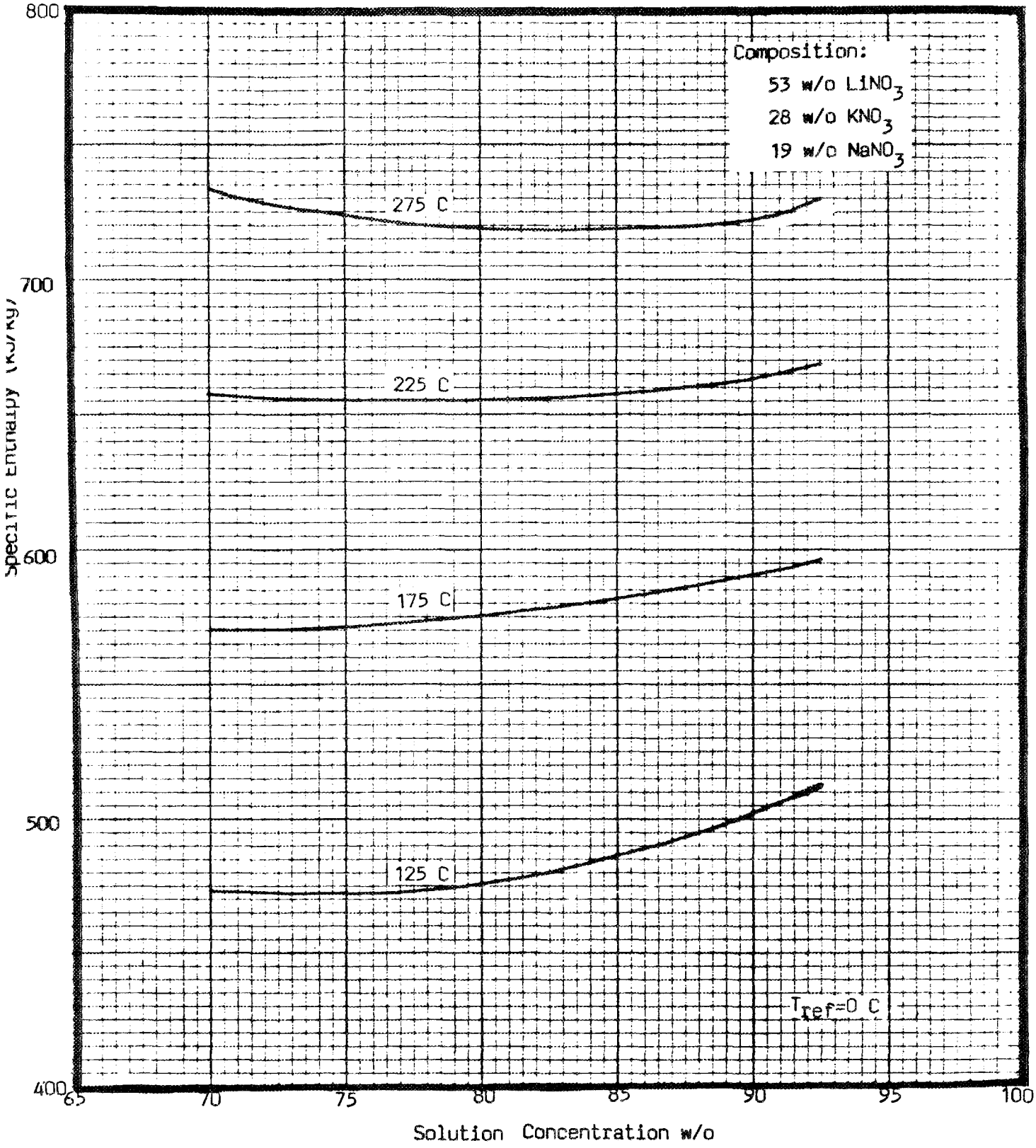

(1968). Comparison of the bromide data provided the basis for calculation of a $LiNO_3$ estimate by invoking an offset below the values for KNO_3. At 80 w/o, for example, this resulted in a conductivity value 24 percent below that estimated for KNO_3.

Most of the literature data are for ambient temperature. However, the effect of temperature is small, and for complex mixtures even less than for than simple liquids (Reid, 1977). Pure water exhibits a 12 percent increase in thermal conductivity from 20°C to 80°C, and remains approxmately constant (varying by less that 2 percent) from 80°C up to 235°C. For the purpose of the present estimate, it was assumed that the temperature dependence of the solution is solely due to the weight fraction of water in the solution.

The three pure nitrate conductivities were combined using the power law recommended by (Reid, 1977):

$$k^{-2} = \sum w_i k_i^{-2}$$

where k = combined thermal conductivity,
k_i = thermal conductivity of species i, and
w = weight fraction of species i.

3.2.2.3. Results

Estimates were calculated for solutions in the following heat amplifier application: 260°C, 86.7w/o generator, and 154.5°C, 83.7w/o absorber. The results were .31 and .33 W/m^2K respectively.

These estimates contain a degree of conservatism due to the extrapolation of pure component data. However, because they are estimated values, not measured, they should not be used with confidence. A plus or minus 30 percent margin is suggested. The next phase of study should include direct measurement of the thermal conductivity of the high temperature absorbent.

3.2.3. Prandtl Number

3.2.3.1 Purpose

Prandtl number is the ratio of momentum diffusion to thermal diffusion. It is the property which links the fluid velocity field with the temperature field in the convective film. This property appears in convective heat transfer relations for estimating film heat transfer coefficients.

3.2.3.2. Method

Prandtl number is defined and calculated as the product of dymamic viscosity and specific heat, divided by thermal conductivity. The first two properties were measured, and the third estimated, all as reported above.

In an absorption heat pump, there are three heat transfer films involving the absorbent. Generator and absorber conditions represent the temperature extremes for the solution as well as the largest components in the solution loop. The solution exchanger experiences intermediate conditions. Therefore, the Prandtl number was calculated for generator and absorber conditions only. Operating conditions for the LiBr system were taken from a LiBr heat pump application, not a chiller. Operating conditions for the high temperature absorbent are postulated as typical for a high temperature heat pump, outside the range of LiBr capability.

3.2.3.3. Results

Table 3.3 presents the results. A Prandtl number of 13 to 23 was calculated for the high temperature absorbent. This compares with 9.8 for LiBr. For the high temperature absorbent, a range is reported to account for a possible 30 percent error in the estimated thermal conductivity values. In heat transfer relations the Prandtl number is typically raised to the 1/3 power, diminishing these differences.

The film heat transfer coefficient is more strongly influenced by thermal conductivity, the property which was estimated, than by any other property reported above. For fully developed flow in a conduit, the ratio of film heat transfer coefficient for the high temperature absorbent, to that for LiBr ranges from .75 to 1.1. (This is using the operating conditions in Table 3.3.) Recognizing the conservatism applied in estimating thermal conductivities (section 3.2.2) this ratio is probably close to 1. For lower temperature heat pumps, where the temperature capabilities of the absorbents overlap, LiBr may have significantly better heat transfer film coeffieients.

Overall surface area requirements are determined by six additional film coefficients: those of the user's fluid and those in the evaporator and condenser. Thus, given the same heat exchanger LMTD's the overall surface area requirements are expected to be similar to those of heat pumps using LiBr.

TABLE 3.3

PRANDTL NUMBER COMPARISON

	Lithium Bromide		High Temp. Absorbent	
	Solution in Generator	Solution in Absorber	Solution in Generator	Solution in Absorber
Typical Conditions:				
Temp. (^{o}C)	160	93	260	154.5
Conc. (w/o)	65	61	86.7	83.7
Viscocity (cP)	2.1	2.5	1.5	3.8
Specific Heat (kJ/kgK)	1.8	2.0	1.8	2.1
Thermal Conductivity* (W/m^2K)	.44	.46	.39±.09	.33±.10
Prandtl Number	8.6	11.	6.8 to 12	19 to 34
Average Prandtl Number	9.8		13 to 23	

* Estimated

4. CORROSION AND THERMAL STABILITY

The two properties addressed in this section are the reason that no other aqueous absorbent to date has successfully been extended to temperatures above about 180°C. Therefore any and all information in this area is highly pertinent and warrants careful scrutiny.

4.1 LITERATURE CITATIONS

The anhydrous alkali metal nitrates are noted for having high stability and resistance to thermal decomposition. When thermal decomposition does occur, both alkali oxides and nitrites are formed, in addition to NOx gases, N_2, and O_2. The temperatures below which thermal decomposition is negligible are given as 650°C for KNO_3, 600°C for $NaNO_3$, and 323°C for $LiNO_3$ (Stern, 1972).

A mixture of approximately 60 w/o $NaNO_3$, 40 w/o KNO_3, known as draw salt, is marketed by several companies as a heat transfer fluid. It is rated as chemically stable up to 595°C (Olin, 1982). There are many instances of industrial use of this salt, for heat treatment as well as for heat transfer. An example of current interest is the Molten Salt Electric Experiment (Holmes, 1983), where 80,000 kg is used at 566°C to store solar energy.

Water vapor is reported to reversibly absorb into and desorb from the $NaNO_3$-KNO_3 mixture at temperatures up to 600°C (White, 1981). Thus the implication is that the presence of water does not induce thermal decomposition to occur at a significantly lower temperature than that at which the anhydrous salt decomposes.

The corrosion behavior of the anhydrous salt has been studied by both DuPont (Kirst, 1940) and by Sandia National Laboratories (Bradshaw, 1982). These references show stainless steels having corrosion rates of less than 1 mil per year at temperatures up to approximately the chemical stability limit, and mild steel at temperatures about 100°C lower. Unfortunately neither $LiNO_3$ containing systems nor aqueous systems were tested. There are, however, two pieces of indirect evidence that the latter systems will also be non-corrosive. First, a certain fraction of the industrial heat transfer systems using nitrate salt incorporate a water dilution system which allows cooldown to ambient temperatures without salt freezeup (Friedman, 1969). The water is boiled out during subsequent heatup, and is essentially all gone by 260°C. This system uses the same mild steel construction as the anhydrous salt systems. Secondly, the alkali metal nitrates are routinely added to aqueous systems as corrosion inhibitors, and $LiNO_3$ is specifically added to LiBr for that purpose.

4.2 EXPERIMENT

Both static isothermal and dynamic temperature cycling tests were conducted. In some corrosion systems this distinction is highly important, as the two types of tests lead to greatly differing results. For the aqueous ternary nitrate system, the results are not significantly different. This is consistent with corrosion data on the anhydrous nitrates reported by Sandia (Bradshaw, 1982), where testing in a thermal convection loop yielded essentially the same results as had been previously reported for static isothermal tests.

Two specimen geometries were used--flat plate and 0.5 inch OD tubing. The typical specimen was 9 inches long, and was immersed approximately three quarters in the absorbent.

The static isothermal tests were conducted in both SS 304 and Inconel 600 pressure vessels, 1 1/2 inch OD by 16 inches long. The solution depth was about 7 inches. A pressure gage was mounted on the vessel. These tests were conducted at various temperatures from 160°C to 310°C, and with various salt compositions, including aqueous $LiNO_3$ alone. The "blank" run, with no corrosion specimen present, was conducted in the Inconel vessel. The dynamic tests were conducted in the same vessel as described above for the above-atmosphere VLE measurement: a 4 inch by 26 inch SS 304 pressure vessel. It was mounted on a shaker, and the temperature continuously cycled from 260°C to 210°C and back at an hourly rate (one hour for each direction). Standard industrial grade alkali nitrate salts were used (Appendix 1). It is considered to be important to conduct this test with salts typical of those which will actually be used industrially, rather than with laboratory grade salts.

The generation of non-condensable gas was monitored over the period of the experiment. The apparatus was evacuated to less than 3 mm Hg absolute pressure at the start while cold, and then the vacuum was measured again while cold at the end. For some experiments, intermediate vacuums measurements were also taken.

When possible, the non-condensable gases were collected and tested. This was difficult, because the amounts were so small, on the order of 10 ml. With the anhydrous salts, it is known that corrosion is accompanied by the release of N_2. For aqueous halides, corrosion results in H_2 generation. The gases collected from the aqueous ternary nitrate neither supported combustion nor would burn, and were colorless. When thoroughly mixed with a small amount of distilled water, a pH of 3.5 was obtained. This evidence is consistent with the gases being a mixture of N_2 and NO. One goal of future research should be the collection of sufficient non-condensables to obtain an accurate analysis of composition.

The pH of the absorbent solution and the condensate were tested after each run. The absorbent typically increased by about 2 units over a 30-day test, e.g., from 6.5 to 8.5. The condensate was usually in the 5.5 to 6 range. This evidence is consistent with a corrosion mechanism whereby alkali

nitrate, metal, and water react to alkali hydroxide, metal oxide, and either N_2 or NO. Note that the presence of both H_2O and NO in the vapor space will cause some nitrous acid to form accounting for the low pH values observed in the condensate.

The appearance of the exposed coupons supports the above hypothesized corrosion mechanism. The solution immersed portions were darkened in color by oxide film formation, but very smooth and obviously passive and well protected. The vapor contact area was also darkened, but not as smooth, and the mild steel specimens showed occasional rust (hematite) colored spots in the vapor exposed area..

Three materials were tested, mild steel (A36), stainless steel (304), and pack aluminized stainless steel. The latter has been found to be effective in resisting anhydrous nitrate corrosion at temperatures above 600°C. The weight change data are presented in Table 4.1, plus the calculated mil/year corrosion rate based on the weight change.

The rate of noncondensable gas generation in the blank run was 4 kPa pressure in 30 days, corresponding to .0018 moles of gas per year. The salt charge was 1.21 moles. Thus the indicated decomposition rate of the absorbent at 315°C is approximately 0.15% per year.

The tabulated data show temperature and $LiNO_3$ content to be the two significant factors in determining corrosion rate, with no apparent effect from water concentration. All of the corrosion rates are extremely low, well within routine industrial tolerance levels. The mild steel does experience noticeably higher corrosion rates than stainless steel, although still very low. As mentioned above, the amount of non-condensable gas generation is also very low, corresponding to the low corrosion rates. The non-condensable gas generated during the blank run was even lower, although it was not zero. It is not known whether the small amount observed was due to slight corrosion of the Inconel vessel or slight decomposition of the absorbent.

One of the mild steel tubing specimens in the cycling experiment was bent and stress loaded before exposure. It had the same resiliency and resistance to further bending after exposure as before, indicating no significant degree of preferential grain boundary attack.

The conclusions to be drawn from the above data are that all stainless steels, including austenitic varieties, are acceptable materials of construction over the entire temperature range; that mild steel is acceptable in absorbent contact areas over the entire temperature range, but should probably not be used in high temperature vapor phase areas (e.g., above 220°C) due to dilute acid attack; and that mildly alloyed steel, e.g., 2.5% Cr, will probably be adequately corrosion resistant in the vapor spaces. It will also probably be necessary to establish a minor liquid bleed rate

from the evaporator to the absorber, on the order of 1/2% of the total condensate flow rate, to prevent excessive concentration of dilute nitrous acid in the evaporator.

TABLE 4.1

AQUEOUS NITRATE CORROSION TESTS

	Specimen Type	Specimen Material	Temperature °C	Duration Days	Sol'n Comp'n w/o	Test Pres. psig	Start Wt. gm	Weight Chg. gm	Noncondens. kPa	mil/year
STATIC	Flat	CS	230	27	Tern. 37 Li	13	73.2	-.02	8	N.C.
	Flat	CS	280	14	Tern. 37 Li	33	63.05	+.15	10	+
	Tube	CS	270	34	Tern. 41 Li	170	76.09	-.19	18	1.06
	Tube	CS	315	34	Tern. 41 Li	270	75.56	-.12	17	0.67
	Tube	Alon SS 304	260	24	$LiNO_3$		104.78	-.58	5	2.84
	Tube	Alon SS 304	260	25	Tern. 53 Li		104.78	+.02	5	+
	Blank		315	30	Tern. 53 Li	100	--	--	4	--
DYNAMIC	Tube	CS	260-210	67	Tern. 53 Li	60-10	218.7	-.02	--	N.C.
	Tube	CS	260-210	20			217.7	-.05	--	N.C.
	Tube	CS	260-210	67			216.95	0.00	--	N.C.
	Tube	CS	260-210	67			99.35	-.01	--	N.C.
	Tube	CS	260-210	67			305.55	0.00	--	N.C.
	Tube	SS 304	260-210	67			129.10	+0.34	--	+

+ = weight gain

N.C. = No significant change

5. ANALYSIS OF PERFORMANCE

5.1. GENERAL

The benefits of an absorption heat pump lie in fuel cost reductions for the user. These stem chiefly from the heat balance of the absorption cycle. From the heat balance can be calculated the heat savings or equivalently the coefficient of performance (COP), which is formally defined below. Using the high temperature absorbent, new industrial applications of heat pumping involving much higher temperatures and significantly higher temperature lifts are possible. The cycle COP and the application temperatures are linked. For higher lifts slightly lower COPs result. This is due to sensible heat effects. Fortunately these effects are not severe, and they can be mitigated with minor additional component design. Another important point, not further treated herein is that the higher temperature energy savings are usually valued higher than the low temperature energy savings associated with present heat pumps.

In the discussion below, both high and low temperature lift cases are assessed with respect to COP. First, the overall temperature and lift capabilities of the high temperature absorbent are presented in comparison with LiBr. Then cycle COP is estimated from basic considerations applying to aqueous absorbents. Finally, COP is rigorously calculated for several cases including a head-to-head comparison with LiBr.

5.2. POSSIBLE USES AND CYCLE DIAGRAMS

Industrial heat pump needs are characterized by variety, particularly with respect to temperature lift requirement and waste heat temperature. A viable heat pumping technology must be capable of satisfying a wide range of temperature lift and waste heat temperature requirements. For any absorption working pair, all feasible cycles can be revealed by careful inspection of the P-T-X diagram, such as Figure 3.5 for the high temperature absorbent. After determining all feasible cycles for a given absorbent from its P-T-X diagram, the temperaure capabilities of those cycles can be summarized using the format of temperature lift vs waste heat temperature. This is the format used in Figures 5.1 through 5.3.

Figure 5.1 illustrates in detail how the capability plot for a single stage heat amplifier is derived. For comparison, the capabilities of LiBr have also been plotted. The P-T-X plot used for LiBr is from ASHRAE (1978) with the crystallization line extended by Pennington (1955) data. Rules for deriving the aplicability plots are applied equally to both absorbents and for both heat amplifier and temperature amplifier modes. They are:

- All heat exchangers have 5.56°C (10°F) LMTD;

FIGURE 5.1

DERIVATION OF HEAT AMPLIFIER APPLICABILITY DIAGRAM

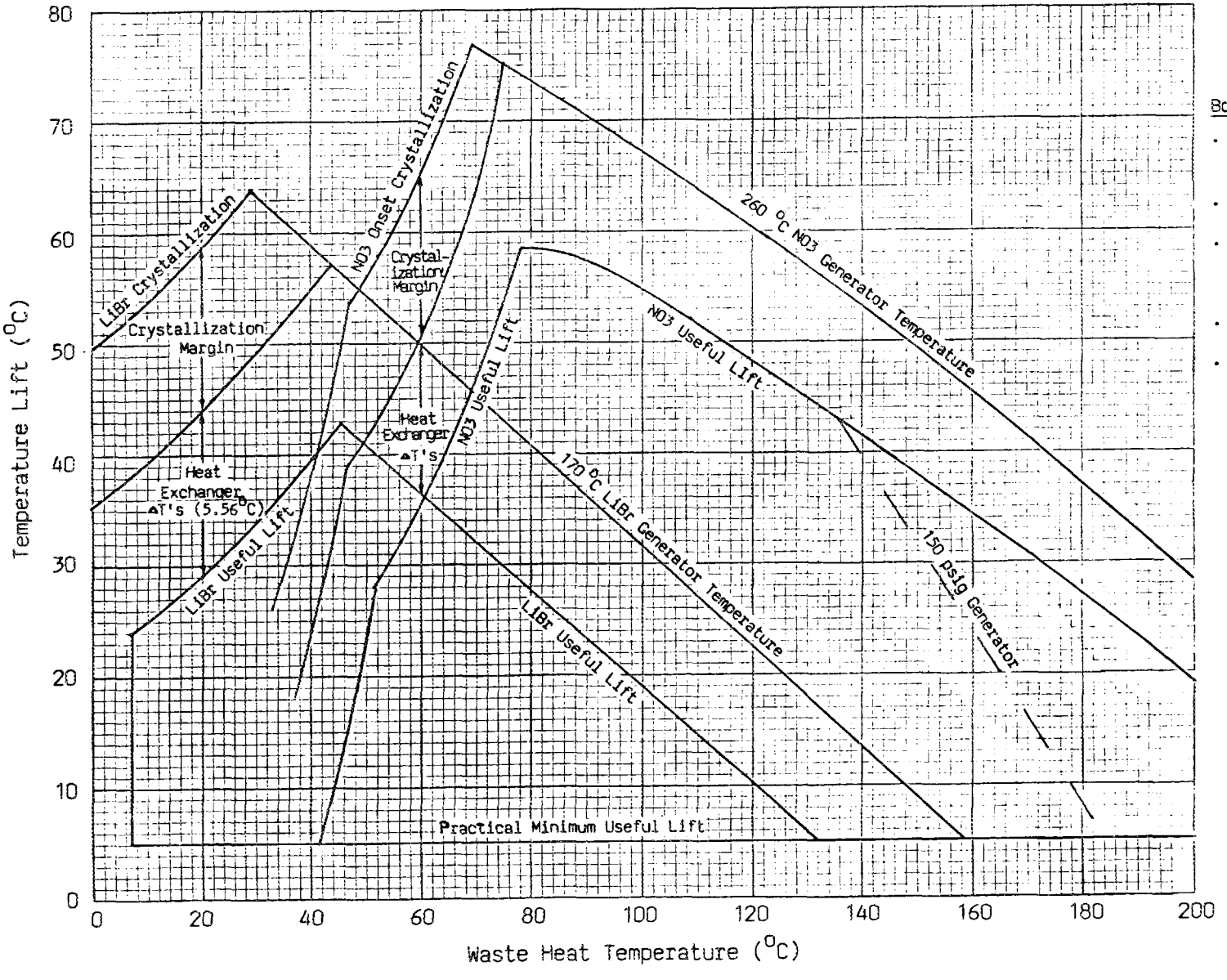

Boundary Definition:

- Heat exchangers have 5.56 °C (10 °F) LMTD
- 3 w/o solution hysteresis
- 15 °C margin to crystallization: constant concentration, or constant pressure
- Nitrate temperature ≤ 260 °C
- LiBr temperature ≤ 170 °C

- 3 w/o solution hysteresis;
- 15°C (27°F) margin against crystallization for both constant concentration cool-down and constant pressure heatup;
- 260°C nitrate solution temperature limit; and
- 170°C LiBr solution temperature limit.

Figures 5.2 and 5.3 show the results for heat amplifier and temperature amplifier modes respectively. Only single stage heat pumps were plotted because these are usually more economic. However, the high temperature capability of the ternary nitrate absorbent also makes possible 2-stage systems for lower lift heat pumping cases where LiBr can provide only a single stage.

Figure 5.2 shows that in comparison to LiBr, the high temperature absorbent can be used in the heat amplifier mode to:

- produce substantially higher useful temperature lifts (up to 58°C vs 43°C), and
- make use of higher temperature waste heat (42°C to above 200°C vs 7°C to 136°C).

Figure 5.3 shows that in comparison to LiBr, the high temperature absorbent can be used in the temperature amplifier mode to:

- produce substantially higher useful temperature lifts (up to 90°C vs 50°C), and
- make use of higher temperature waste heat (60°C to 240°C versus 55°C to 155°C)

Also, comparing the two figures shows that the applicability field for the high temperature absorbent used in the heat amplifier mode completely overlaps the applicability field for LiBr used in the temperature amplifier mode. This is important in cases where cooling water is limited and where the temperature amplifier would require additional cooling water.

As noted above, wide applicability is the hallmark of a successful industrial heat pumping technology. The applicability diagrams show that for both the heat amplifier and temperature amplifier modes, the high temperature absorbent is much more widely applicable (area under the curves) than current technology.

FIGURE 5.2
HEAT AMPLIFIER APPLICABILITY DIAGRAM

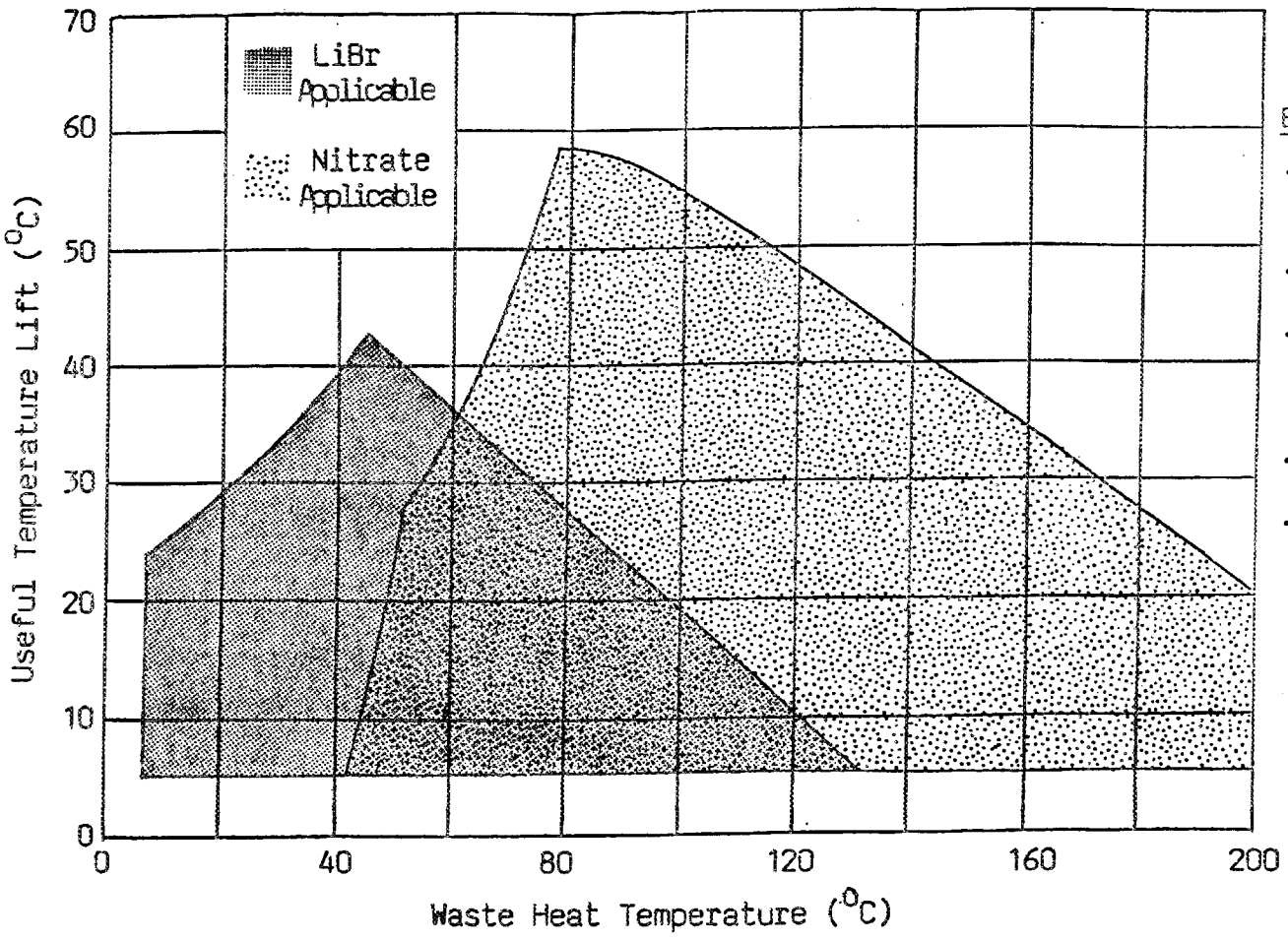

Boundary Definition:

- Heat exchangers have 5.56 °C (10 °F) LMTD
- 3 w/o solution hysteresis
- 15 °C margin to crystallization: constant concentration, or constant pressure
- Nitrate temperature ≤ 260 °C
- LiBr temperature ≤ 170 °C

FIGURE 5.3

TEMPERATURE AMPLIFIER APPLICABILITY DIAGRAM

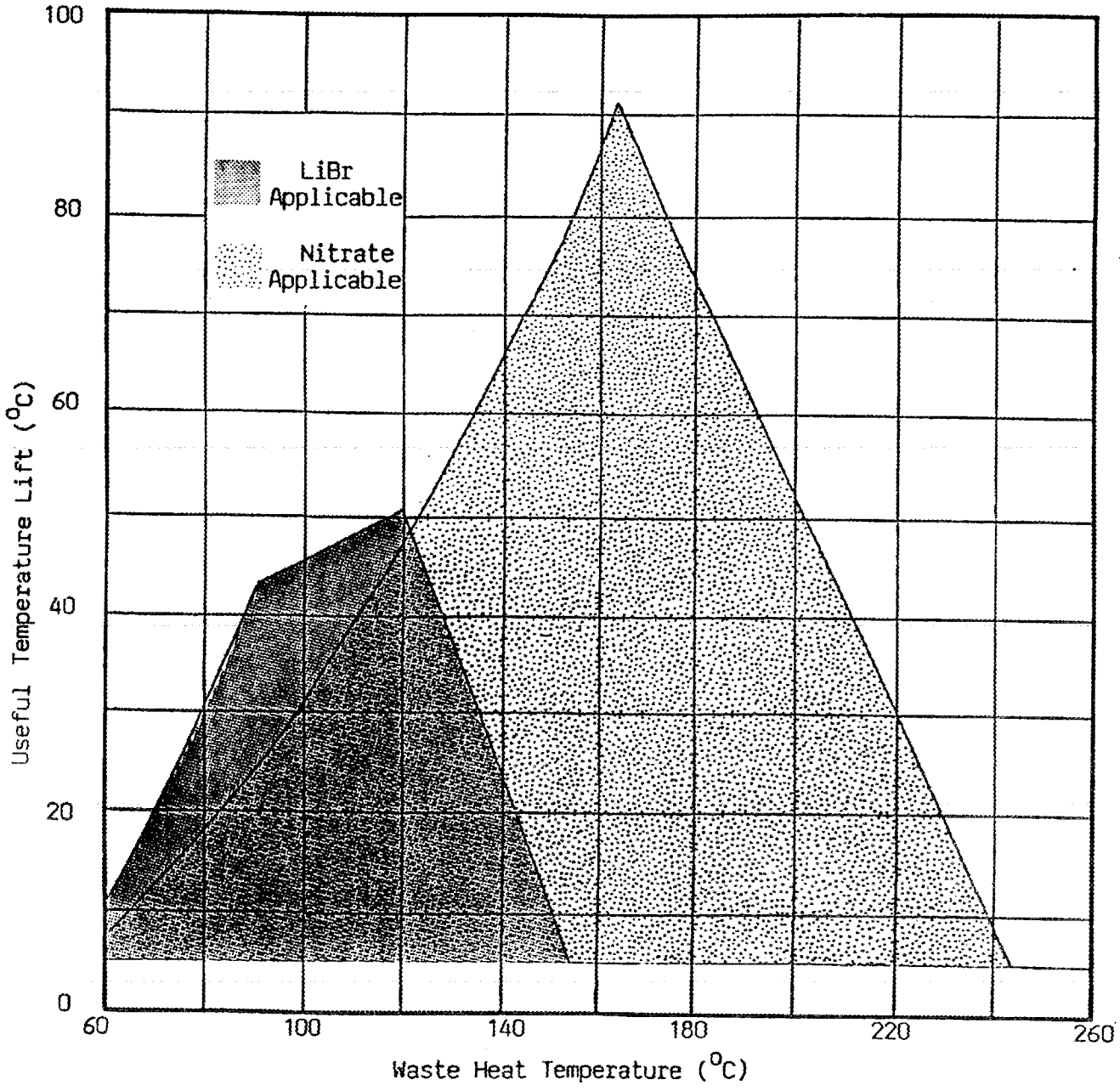

Boundary Definition:

- Heat exchangers have 5.56 °C (10 °F) LMTD
- 3 w/o solution hysteresis
- 15 °C margin to crystallization: constant concentration, or constant pressure
- Nitrate temperature ≤ 260 °C
- LiBr temperature ≤ 170 °C

5.3. ESTIMATION OF COP

The COP of an absorption heat pump can be estimated from P-T-X data alone. This should routinely be done when screening new absorbents. It also provides corroboration for detailed analytical results.

The heat amplifier COP for the ternary nitrate was estimated by the following procedure: considering only phase change thermodynamics, and ignoring heat exchanger losses

$$COP_{ideal} = \frac{\Delta Ha + \Delta Hc}{\Delta Hg}$$

It may be assumed that

$$\frac{\Delta He}{\Delta Ha} = \frac{\Delta Hc}{\Delta Hg} = \frac{\Delta H^{o}_{H2O}}{\Delta H^{o}_{sol'n}}$$

This relation holds when reduced temperatures scale linearly with boiling points, based on the Watson correlation (Watson, 1943). Thus,

$$COP_{ideal} = \frac{\Delta Ha}{\Delta Hg} + \frac{\Delta Hc}{\Delta Hg}$$

$$= \frac{\Delta He}{\Delta Hc} + \frac{\Delta H^{o}_{H2O}}{\Delta H^{o}_{sol'n}}$$

For typical condenser and evaporator temperatures, $\Delta He / \Delta Hc = 1.088$.

The ΔH^{o}_{H2O} at 1 atmosphere is 9.178 kcal/gmole, and for the 85 w/o concentration

$$\Delta H^{o}_{H2O} / \Delta H^{o}_{sol'n} = 1.088$$

and the $COP_{ideal} = 2.176$.

The ideal COP represents the limiting performance under very high solution pumping rates and with infinite heat exchange. At the other extreme, under high pumping rates and with no heat exchange, the limiting COP is 1. A reasonable design point for an actual machine is to achieve 70% of the heat exchange ideally possible. Under that assumption:

$$COP_{est.} = 1 + (COP_{ideal} - 1)(0.70)$$

$$= 1.82$$

5.4 CALCULATION OF COEFFICIENT OF PERFORMANCE

5.4.1. Definitions

For absorption heat pumping the heating COP (COP_h) is defined as the ratio of useful heat output divided by the high grade heat input (as distinguished from the waste heat input). To account for parasitic pumping power, a net measured COP (COPnm) is defined as follows:

Net measured COP:

For Temperature Amplifier:

$$COP_{nm} = \frac{\text{Heat Delivered}}{\text{(Heat Extracted From Input Stream Plus 4 x Pumping Power)}}$$

For Heat Amplifier:

$$COP_{nm} = \frac{\text{Heat Delivered}}{\text{(Heat Input From Driving Source Plus 4 x Pumping Power)}}$$

Pumping power is calculated by applying a 65% efficiency to the calculated ideal pump work.

5.4.2. Example Calculation of COP

In the examples below it can be seen that the net measured COP is always only 1 or 2% lower than the heating COP. This is due to the extremely high latent heat of evaporation of water, and the resulting low absorbent circulation rates, compared to any other working fluid. Thus the distinction between heating COP and net measured COP is generally not significant for this high temperature absorbent.

Energy balances were calculated for the example cycles depicted in Figures 5.4 and 5.5. This was done using the NBS Steam Tables (Haar, 1984) and Figure 3.8, the Merkel diagram for the high temperature absorbent. The calculated temperatures, enthalpies, and mass flow rates are shown on the figures.

Figure 5.4 presents a thermodynamic cycle diagram and flowsheet for an example of a heat amplifier using the high temperature absorbent. This closed cycle heat pump produces 53 psig steam from atmospheric pressure waste steam, such as from a wort boiler at a brewery. In this example the generator temperature has been limited to 247°C. This heat pump could produce higher pressure steam from the same

FIGURE 5.4

HEAT AMPLIFIER WITH HIGH TEMPERATURE ABSORBENT

Function: Produces 53 psig Steam From Atmospheric Steam

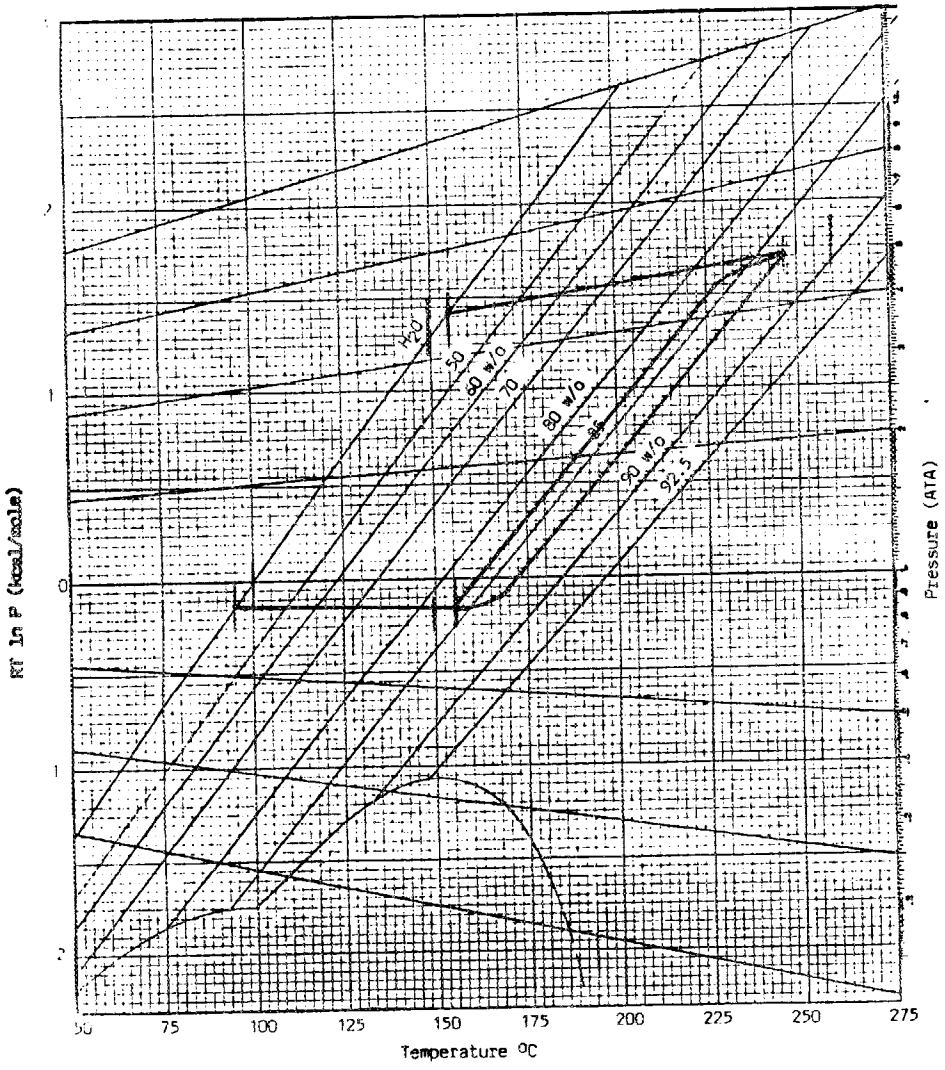

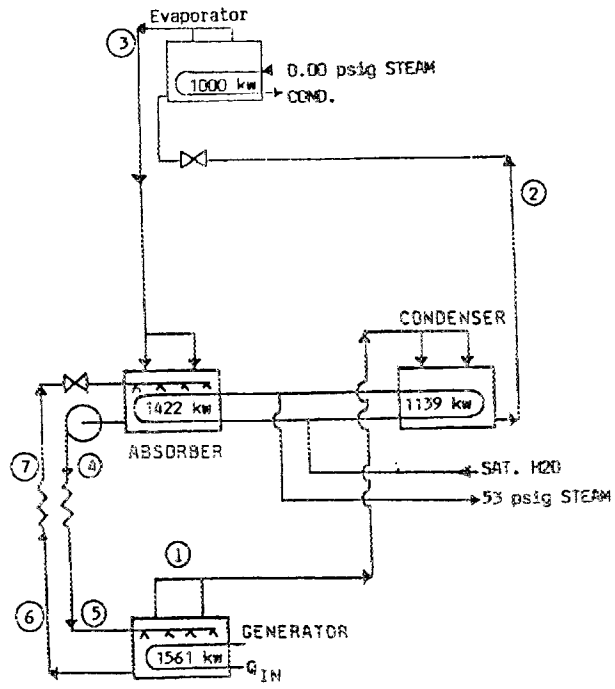

STREAM NO.	FLUID DESCRIPTION	TEMP. C	PRES. ATA	CONC. W/O SALT	ENTHALPY KJ/kg	FLOW kg/s
1	STM. FROM GEN.	247.0	5.22	0.0	2949	0.496
2	WTR. FROM COND.	154.5	5.22	0.0	652	0.496
3	STM. FROM EVP.	95.0	.823	0.0	266.8	0.496
4	SOL. FROM ABS.	154.5	.823	83.7	541.0	14.33
5	SOL. TO GEN.	225.1	5.22	83.7	655.4	14.33
6	SOL. FROM GEN.	247.0	5.22	86.7	686.0	13.84
7	SOL. TO ABS.	164.5	.823	86.7	567.5	13.84

COP = 1.64

Figure 5.5

TEMPERATURE AMPLIFIER WITH HIGH TEMPERATURE ABSORBENT

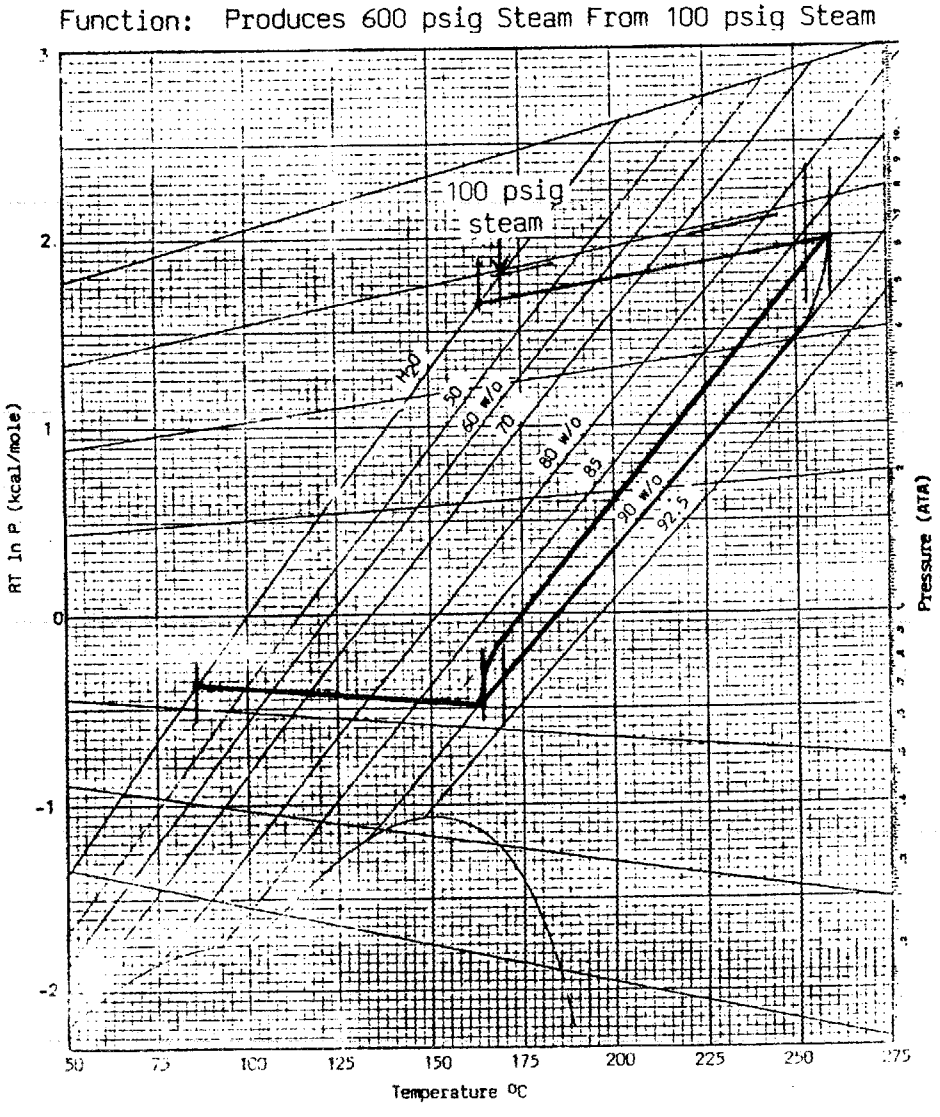

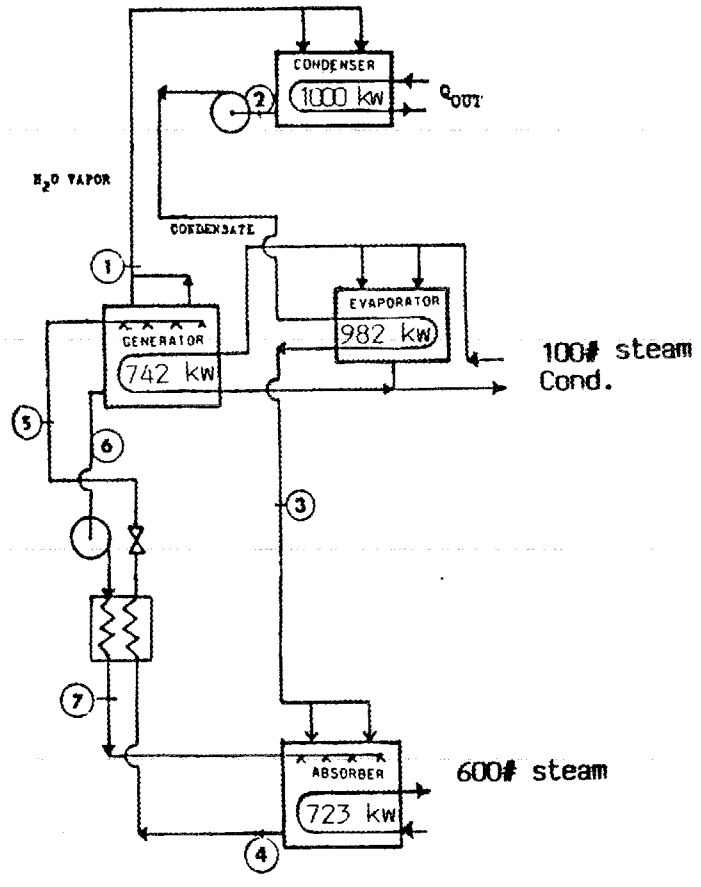

OPERATING PARAMETERS

STREAM NO.	FLUID DESCRIPTION	TEMP. C	PRES. ATA	CONC. W/O SALT	ENTHALPY KJ/kg	FLOW kg/s
1	STM. FROM GEN.	164.4	.5933	0	2807	.409
2	WTR. FROM COND.	86.0	.5933	0	360	.409
3	STM. FROM EVP.	164.4	6.80	0	2763	.409
4	SOL. FROM ABS.	260.0	6.80	87	702	12.26
5	SOL. TO GEN.	174.4	.5933	87	585	12.26
6	SOL. FROM GEN.	164.4	.5933	90	571	11.85
7	SOL. TO ABS.	250.0	6.80	90	691	11.85

COP = .420

atmospheric waste steam if the generator temperature is increased.

Figure 5.5 presents a thermodynamic cycle diagram and flowsheet for an example of a temperature amplifier using the high temperature absorbent. This absorption heat pump produces 600 psig steam from 100 psig waste steam. The condenser temperature is high enough to allow economic disposal of low grade heat to the atmosphere via fin tubes instead of adding burden to the cooling water utilities. This example demonstrates the extreme of high lift and high temperature capability. Note that for the same advantageous condenser temperature, 50 psig waste steam can be raised to 250 psig steam.

These flowsheets represent preliminary estimate designs; no attempt was made to optimize design parameters such as solution concentration hysteresis or solution heat exchanger approach temperatures. Also, these designs include no sensible heat recovery from the working fluid as would be appropriate for high lift cases. The results for these simple cases are as follows:

The COP_h and COP_{nm} for the heat exchanger example depicted in Figure 5.2 are 1.64 and 1.61 respectively.

The COP_h and COP_{nm} for the temperature amplifier example depicted in Figure 5.3 are 0.42 and 0.41 respectively.

It should be noted that including two very small sensible heat exchangers increases the amount of useful heat delivered by approximately 6 percent. In the heat amplifier, these exchangers would (1) heat up dilute solution by desuper heating steam from the generator, and (2) superheat steam from the evaporator by subcooling water from the condenser. In the temperature amplifier the sensible heat exchangers would (1) cool dilute solution by superheating steam from the evaporator, and (2) heat water from the condenser by desuperheating steam from the generator. These minor hardware additions become more economic for higher temperature lifts.

5.4.3. Comparison with LiBr

The cycles assessed above cannot be achieved with LiBr. For a meaningful comparison to LiBr, the application depicted in Figure 5.6 was chosen. This heat amplifier is achievable with both LiBr and the high temperature absorbent. Two flowsheets were calculated--one for each absorbent. In each case the design parameters were identical: closed cycle, no sensible heat exchange of the working fluid, 3.0 w/o solution concentration change, and 5.6°C solution heat exchanger temperature approach. The calculated COP_h is 1.81 with LiBr versus 1.87 with the high temperature absorbent. Calculated parasitic power is insignificant for both cases due to the low temperature lift; the $COP_{nm} \approx COP_h$. The high temperature

FIGURE 5.6

COP COMPARISON EXAMPLE

High Temperature AWP

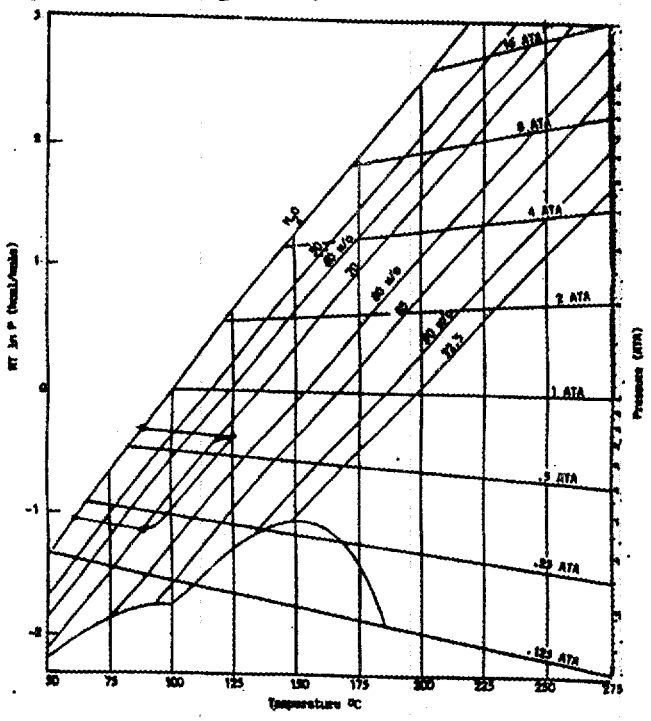

H_2O-LiBr

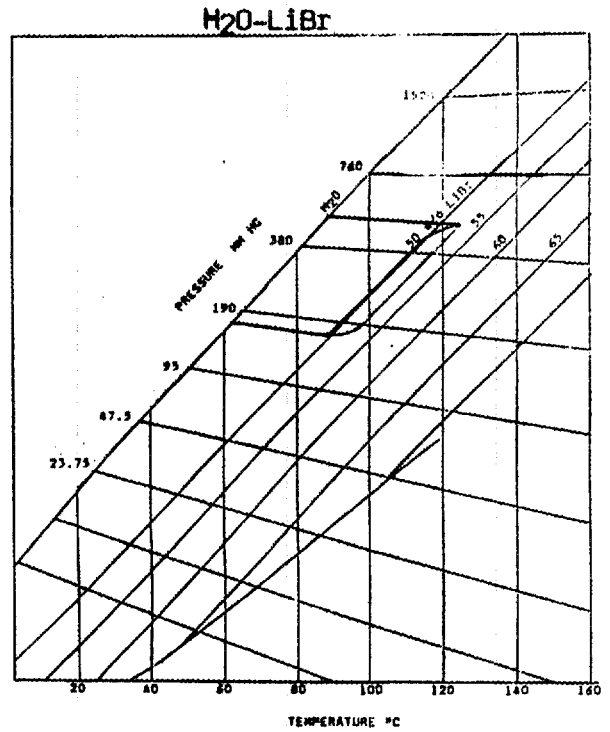

Heat Amplifier Flowsheet

61.2°C EVAP.
88.5°C COND.

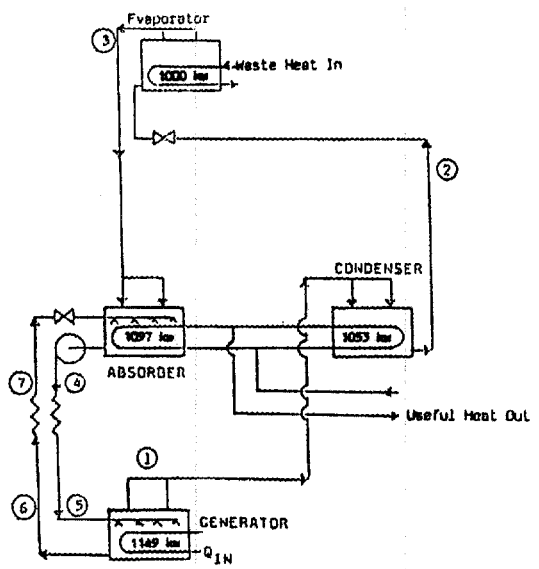

High Temperature AWP

TEMP. C	Pres. ATA	CONC. W/O SALT	ENTHALPY KJ/kg K	FLOW kg/s
125.0	.5820	0	2730	.444
88.5	.5820	0	358	.444
61.2	.2079	0	2611	.444
88.5	.2079	70	397.5	10.80
119.3	.5820	70	459.4	10.80
125.0	.5820	73	473.1	10.36
94.1	.2079	73	408.5	10.36

COP 1.87

LiBr

STREAM NO.	FLUID DESCRIPTION	TEMP. C	PRES. BAR	CONC. W/O SALT	ENTHALPY KJ/kg	FLOW kg/s
1	STM. FROM GEN	125.1	.6623	0	2731.	5.85
2	WTR. FROM COND.	88.5	.6623	0	369.8	5.85
3	STM. FROM EVP.	61.2	.2107	0	2612.	5.85
4	SOL. FROM ABS	88.5		49.8	118.9	103
5	SOL. TO GEN	116.7		49.8	251.7	103
6	SOL. FROM GEN	125.1	.6623	52.8	269.1	97.2
7	SOL. TO ABS	94.1		52.8	202.6	97.2

COP 1.81

absorbent has a 3.3% higher COP than LiBr in the heat amplifier mode.

An additional example was calculated, but not illustrated, at a useful temperature lift of 45°C. Both COPs degenerated (without additional sensible heat exchangers), but the high temperature absorbent retained a 2.2 percent COP advantage.

These results are consistent with the fact that the high temperature absorbent exhibits less negative deviation from Raoultian behavior than does LiBr. As a general rule, for equivalant system designs, the heat amplifier COP using the high temperaure absorbent will be slightly better than that of LiBr in the same cycle conditions. Correspondingly, the temperature amplifier COP will be slightly less than that of LiBr. However, the scale and temperature lifts of the new industrial applications now made feasible will often justify the addition of the small sensible heat exchangers noted above for enhanced COPs in both cycles.

6. CONCLUSIONS

The newly identified water vapor absorbent has successfully passed all the laboratory tests intended to check its suitability as a high temperature absorbent for absorption heat pumping. At temperatures of 260°C and higher the absorbent

- has negligible thermal decomposition
- has corrosion rates less than 1 mil/year for both carbon steel and austenitic stainless steel
- provides practical heat pumping lifts of up to 90°C.

The absorbent is useful for waste heat temperatures as low as 60°C, and with corresponding absorbent temperatures ranging from 100 to 260°C. Over that range, the absorbent thermodynamic properties are at least as good as the corresponding values in currently operating LiBr units.

The new absorbent is not a panacea for all existing absorbent limitations. It cannot replace LiBr in air conditioning applications, nor NH_3-H_2O in refrigeration applications. It should not be expected that the high temperature absorbent will replace LiBr in all industrial heat pumping applications. Rather, there is a complementary relationship with LiBr. In addition to unique applicability areas, LiBr has slightly better COPs in the temperature amplifier mode in the area of applicability overlap, and LiBr may have better heat transfer properties for low temperature applications. For the higher lifts the high temperature absorbent requires either a shutdown dilution system or a separate melt tank. It does, however, greatly extend the existing capabilities of absorption heat pumps. Maximum

useful lift is increased from 50 to 90°C, and maximum absorbent temperature is increased from 170 to 260°C. This extension in capabilities brings many important industrial applications within the scope of absorption heat pumping for the first time.

7. RECOMMENDATIONS

It is recommended that this research proceed to the pilot plant stage, to demonstrate cycle performance and determine heat and mass transport properties, particularly absorption rates. Supportive laboratory work is also recommended to:

(1) extend specific heat measurements;
(2) test mildly alloyed steels plus copper alloys for corrosion;
(3) analyze non-condensable gases from corrosion;
(4) directly measure thermal conductivity; and
(5) establish specific metallurgical requirements, tolerances, and code requirements.

8. ACKNOWLEDGEMENTS

The assistance of the University of Maryland in performing the vacuum VLE and specific heat measurements, plus general support on other tasks, is gratefully acknowledged. The work was performed by Wei-Chu Li and John Zhang under the direction of Dr. Reinhard Radermacher.

9. REFERENCES

ASHRAE. 1977. Fundamentals Manual. New York, New York.

Barin, I., and O. Knake. 1973. Thermochemical Properties of Inorganic Substances. Springer-Verlag, Berlin, Germany.

Bradshaw, R. W. 1982. "Thermal Convection Loop Corrosion Tests of 316SS and IN800 in Molten Nitrate Salts". Sandia Report, SAND081-8210. Sandia National Laboratories, Albuquerque, New Mexico.

Braunstein, Helen and J. Braunstein. 1971. "Isopiestic Studies of Very Concentrated Aqueous Electrolyte Solutions of LiCl, LiBr, $LiNO_3$, $Ca(NO_3)_2$, $LiNO_3 + KNO_3$, $LiNO_3 + CsNO_3$, and $Ca(NO_3)_2 + CsNO_3$ at 100 to 150°C". J. Chem. Thermodynamics. Vol. 3. New York, New York.

Dewing, Ernest W. 1975. "Heat Capacities of Liquid Sodium and Potassium Nitrates" Journal of Chemical and Engineering Data, Vol. 20, No. 3. American Chemical Society. Washington, D. C.

Duran, M. A. and I. E. Grossmann. 1986. "Simultaneous Optimization and Heat Integration of Chemical Processes". AIChE Journal, Vol. 32, No. 1. New York, New York.

Erickson, Donald C. 1983. "Oxygen Production by the Moltox™ Process". DOE/CS/40287-T2 (DE83012847). U.S. Department of Energy, Washington, D.C.

Fiorucci, L. C. and S. L. Goldstein. 1982. "Manufacture, Distribution, and Handling of Nitrate Salts for Solar Thermal Applications". SAND81-8186. Sandia National Laboratories, Albuquerque, New Mexico.

Friedman, Joel and Alfred Bruhn. 1969. "Salt for Indirect Heating" Industrial Gas. American Hydrotherm Corporation, New York, New York.

Haar, Lester, J. S. Gallagher and G. S. Kell. 1984. NBS/NRC Steam Tables Hemisphere Publishing Corporation, New York, New York.

Haltenberger, William, Jr. 1959. "Enthalpy-Concentration Charts from Vapor Pressure Data". Industrial and Engineering Chemistry. American Chemical Society. Washington, D.C.

Holmes, John T. 1983. "The Solar Molten Salt Electric Experiment" SAND83-1021 C. Sandia National Laboratories, Albuquerque, New Mexico.

Hougen, Olaf A. and Kenneth M. Watson. 1943. Chemical Process Principles Part I. John Wiley & Sons, Inc., New York, New York.

Ichikawa, K. and Matsumoto, T. 1983. Bull Chemical Society of Japan. Vol. 56. No. 2093.

Inman, Douglas and David G. Lovering. 1981. Ionic Liquids Plenum Press, New York, New York.

Kirst, W. E., et al. 1940. "A New Heat Transfer Medium for High Temperatures". Transactions of AIChE No. 36. AIChE. New York, New York.

Landolt, Hans Heinrich. 1968. Landolt-Bornstein Zahlenwerte und Funktionen. Springer-Verlag. New York, New York.

Marchidan, D. I. and Telea, C. 1968. Rev. Roumaine Chim. Vol. 13 No. 1291.

McNeely, Lowell A. 1979. "Thermodynamic Properties of Aqueous Solutions of Lithium Bromide". ASHRAE Transactions #85. ASHRAE. Atlanta, Georgia.

Olin Chemicals. 1982. "Olin Heat Transfer Salt 222" Olin Chemicals, Stamford, Connecticut.

Parker, Vivian Barfield. 1965. "Thermal Properties of Aqueous Uni-univalent Electrolytes", National Standards Reference Data System, National Bureau of Standards. Washington, D. C.

Pennington, W. A. 1955. Refrigeration Engineering. 63. Atlanta, Georgia.

Puchkov, L. V., R. P. Matveeva, and T. L. Baranova. 1973. "Specific Heats of Aqueous Solutions of Sodium and Potassium Nitrates at Temperatures in the Range 25-340°C". Journal of Applied Chemistry. Vol. 46, No. 460. USSR (Eng. Trans.).

Reid, R. C., Prausnitz, J. M., and Sherwood, T. K. 1977. The Properties of Gases and Liquids. McGraw Hill Book Company. New York, New York.

Stern, Kurt H. 1972. "High Temperature Properties and Decomposition of Inorganic Salts" Part 3. Journal of Physical and Chemical Reference Data. Vol. 1, No. 3. National Bureau of Standards, Washington, D. C.

Vargaftik, N. B. 1975. Handbook of Physical Properties of Liquids and Gases. Hemisphere Publishing Corporation. New York, New York.

Watson, K. M. 1943. "Thermodynamics of the Liquid State". Industrial and Engineering Chemistry.

White, S. H. and U. M. Twardoch. 1981. "A Study of the Interactions of Molten Sodium Nitrate-Potassium Nitrate 50 Mol % Mixture with Water Vapor and Carbon Dioxide in the Air". EIC Laboratories, Inc., Newton, Massachusetts

Winkelman, A., 1873. Annalen Der Physik und Chemic. Ann. Phys. Vol. 149, No. 1. Liepzig, Germany.

Lithium Nitrate

$LiNO_3$
A white, hygroscopic, crystalline powder

CAS Registry No. 7790-69-4

LITHCO
Lithium Corporation of America
449 North Cox Road
Gastonia, North Carolina 28052
(704) 867-8371
Telex 57-5253

Chemical Analysis

	Typical (%)	Guaranteed (%)
$LiNO_3$	99.5	99.0 min
H_2O	0.5	1.0 max
Alkalinity (as Li_2CO_3)	0.02	0.05 max
SO_4	0.01	0.05 max
Cl	0.003	0.01 max
Fe_2O_3	0.002	0.005 max

Physical Analysis

Bulk density 1.4 g/cm³ (90 lb/ft³)

Properties

Molecular weight	68.95
Density	2.366 g/cm³ at 20°C
Melting point	251.4°C
Decomposition temperature	600°C
Specific heat	0.387 cal/g/°C at 210°C
Standard heat of formation	-115.279 kcal/mole
Heat of solution	-.333 kcal/mole at 18°C
Water solubility	43 wt. % at 20°C

APPENDIX 1

CHEMICAL ANALYSIS OF INDUSTRIAL GRADE KNO_3

Supplier Grade	Vertac Chemical Tech Crystal
$NaNO_3$	0.410
KNO_3	99.38
Nitrite	0.005
Chloride	0.012
Sulfate	0.088
Calcium	0.0027
Magnesium	0.0029
Silica	0.010
Copper	0.0001
Iron	0.0020
Carbonate	0.0741
Hydroxide	0.001
Hot Water-Insoluble	0.0126
Aluminum	0.0005
Chromium	0.0003
Nickel	0.0002
Moisture	0.087

Source: Foirucci, 1982

Olin INORGANIC CHEMICALS

PRODUCT DATA

SODIUM NITRATE

Olin sodium nitrate, $NaNO_3$, is manufactured in Lake Charles, Louisiana. It is in the form of hard spherical pellets with a bulk density of 80 pounds per cubic foot and it is prilled to provide a uniformly free-flowing material with minimum dusting properties. These qualities are maintained over long periods in storage. Specifications for Olin sodium nitrate are given in Table 1.

Table 1
Specifications

Component	Shipping Limit (%)
$NaNO_3$, min	99.4
$NaNO_2$, max	.025
NaCl, max	.25
Na_2SO_4, max	.40
SiO_2, max	.0085
CaO, max	.03
MgO, max	.002
Al_2O_3, max	.001
Mn, max	.0001
Cu, max	.0001
I, max	.0001
Fe_2O_3, max	.0025
H_2O, max	.02
Hot Water Insolubles, max	.03
Total Methyl Orange Alkalinity as Na_2CO_3, max	.04
Total N, min	16.3

Principal Uses

Sodium nitrate is used in the manufacture of explosives, glass, ceramics, pyrotechnics, soaps and detergents, charcoal briquettes, pulp and paper and porcelain enamel. It is used as a fertilizer and in fertilizer mixtures and has a number of other chemical uses. Metallurgical industries use sodium nitrate as a flux, as an oxidizing agent and as a component in heat treating baths.

In bags coded food grade, Olin sodium nitrate is acceptable to the Meat Inspection Division of the United States Department of Agriculture as a color fixing agent in meat curing.

Table 2
Screen Analysis

U.S. Standard Screen	%
On 6 mesh, max	1
Thru 6, on 20 mesh, min	50
On 60 mesh, min	96
Thru 100 mesh, max	1.5

Toxicological Properties

The acute oral LD_{50} for sodium nitrate is 4.3g/kg. Sodium nitrate is considered toxic from this route of exposure according to criteria established by the Federal Government in the Hazardous Substances Act. No information is available on the toxicity from dermal or inhalation exposure but, in all probability, it would not be considered toxic from either of these routes of exposure. Sodium nitrate may be a skin irritant and an eye irritant. Sodium nitrate will not present a hazard to health when used according to normal industrial handling practices.

Personnel Protection

Use with adequate ventilation. Wear goggles, coveralls and impervious gloves and boots.

Spill and Leak Procedure

Remove all sources of ignition. Wear a NIOSH/MSHA approved dust respirator. Follow OSHA regulations for respirator use. (See Chapter 29, *Code of Federal Regulations* 1910.134.) Wear goggles, coveralls and impervious gloves and boots. Minimize contamination with organic material. Do not return to original container. Place in a fresh container and isolate outside or in a well ventilated area. Do not seal container. Flush any residual material with large quantities of water. Wash off contaminated clothing before reuse.

Disposal

Dispose of unused product in a manner approved for this material. Consult appropriate Federal, state and local regulatory agencies to ascertain proper disposal procedures.

Shipping

Olin sodium nitrate is shipped in 50- and 100-pound, 5-ply, polyethylene-lined paper bags. Unitized bag ship-

Olin CHEMICALS
120 Long Ridge Road, Stamford, Connecticut 06904

© 1981 Olin Corporation

MEASURED VLE DATA

Concentration w/o Salt	Temperature °C	Pressure -mm Hg	Concentration w/o Salt	Temperature °C	Pressure -mm Hg
50	40	727	78	80.2	693
	50	704		90	657
	60	670		100	609
	70	621		110	544
	80	548		120	466
	90	450		130	353
	100	318		140	211
	110	142		151	-4
	115.5	0			
60	40	734	80	90	682
	50	715		100	642
	60	691		110	587
	70	653		120	515
	80	592		130	421
	90	504		140	302
	100	409		150	144
	110	269		157.6	0
	120	84			
	123.8	0			
65	55	714	82.6	110	619
	60	701		120	549
	70	667		130	480
	80	619		140	367
	90	556		150	240
	100	470		160	80
	110	352		164	0
	120	190			
	129	-4			
70	50	731.8	87	131.4	541
	60	712.4		140	460
	70	682.7		150	360
	80	644.1		160	237
	90	584.6		170	72
	100	507.3		174.5	-3
	110	407.3			
	120	277			
	130	94.1			
	133	0			
76	70	708	88	130	560.6
	80	679		140	483.6
	90	636		150	392.6
	100	582		160	272.6
	110	508		170	108.6
	120	413		176.5	0.6
	130	263			
	140	104			
	144	6			

MEASURED VLE DATA

Concentration w/o Salt	Temperature °C	Pressure -mm Hg
92.4	156	479
	160	450
	165	404
	170	354
	175	307
	180	240
	185	164
	190	88
	195	3
	195.5	-9
94.1	170	453
	175	401
	180	356
	185	295
	190	241
	195	176
	200	108
	205	21
	206.7	3

Concentration w/o Salt	Temperature (°C)	Pressure psig
80	164.5	12.5
	151	3.6
	147	1.0
	150	0.9
	157	5.0
	163	9.0
	170	12.9
	172	14.5
	171	14.2
	178	20.1
	190	32.1
	197	40.0
	207	55.0
	211	61.6
	232	101.2
	238	115
84.9	186	11.9
	164	0.7
	188	14.0
	203	27.4
	212	37.2
	234	59.3
	236	70.0
	249	90.0
	260	114
	269	134
	278	156.5
	248	98.2
89.7	186	1.2
	199	8.1
	221	24.3
	239	38.2
	248	48.8
	252	53
	213	68.5
	274	84
	289	110
	303	137.5
	312	160
	303.5	134.5
	289	107
	280	93.0
	274	81
	262	63
	256	56
	253	52.2

APPENDIX 3

CALCULATIONS FOR CONSTRUCTION OF THE MERKEL DIAGRAM

Construction of the enthalpy-concentration-temperature plot, called a Merkel diagram, followed the technique used by McNeely for aqueous LiBr (McNeely, 1985). The intermediate calculations are displayed in Table A3.

Nomenclature

x = concentration (w/o) of solution

dt/dt' = slope of Duhring plot, also ratio of Clapeyron equations

t' = temperature (^{o}C) of saturated water at P

t = temperature (^{o}C) of solution at P

P = pressure (bar)

$\Delta H'$ = latent heat (kJ/kg) of water at t'

V' = specific volume (m^3/kg) of saturated water vapor at t'

V = specific volume (m^3/kg) of superheated water at t and P

ΔH = latent heat (kJ/kg) of solution

H_v = enthalpy (kJ/kg) of superheated water at t and P

$\bar{H}$ = partial enthalpy of water in solution

$w = (1 - x/x_o)$ = water (kg) added or subtracted to change from x_o to x

x_o = 80 (w/o)

$H_o = \int_{t_o}^{t} Cp\, dt$ = enthalpy (kJ/kg) of base solution at t

Cp = specific heat (kJ/kg) at x and t

H_l = saturated solution liquid enthalpy (kJ/kg K) at x and t

The Duhring diagram in the text provided the water and corresponding solution saturation temperatures, t, and t'. The NBS steam tables (Haar, 1984) provide all values for water.

Specific heat data for a single concentration was necessary. The specific heat test data for 80 w/o was used.

Solution enthalpies were calculated for 20 data points: four solution temperatures, 125 ^{o}C, 175 ^{o}C, 225°C, and 275°C, and for five concentrations ranging from 70 w/o to 92.5 w/o. These calculations used the following four equations:

$$\Delta H = \frac{\Delta H' \; V(273.15 + t)}{(dt/dt') \; V' \; (273.15 + t')} \tag{1}$$

$$\overline{H} = H_v - \Delta H' \tag{2}$$

$$H_o = \int_{100}^{t} Cp \; dt \tag{3}$$

$$H_i = \frac{H_o - \int_{x_o}^{x} \overline{H} \; d(1 - x_o/x)}{x_o / x_i} \tag{4}$$

Equation (1) results from the ratio of two Clapeyron equations, one for the solute, one for the solvent, at the same pressure. The parameter (dt/dt') is the slope of the Duhring line for a given concentration.

Equation (2) states the definition that the partial enthalpy of water in solution is the difference between the enthalpy of its vapor and the latent heat of the water.

Equation (3) states the definition of specific heat. It was applied to the 80 w/o concentration. Note that the reference state of 100°C was chosen for this purpose. Specific heat for 80 w/o solution temperatures below 100°C was not measured. (This solution crystallizes at approximately 75°C.) The relation used was: $Cp = 3.1642 - .007707T^{o}C$.

Equation (4) was derived by Haltenberger (Haltenberger, 1939) from a heat and mass balance for isothermal evaporation of water from a solution. The integration required for equation 4 was accomplished graphically with the aid of Figure A3.

The final tabulated values for solution enthalpy, H_i, were increased by 419.06 kJ/kg for plotting of the Merkel diagram. This was to correspond to the conventional reference state for water, and to simplify use of the diagram.

FIGURE A3

PARTIAL ENTHALPY OF WATER H IN SOLUTION VS. WATER ADDED

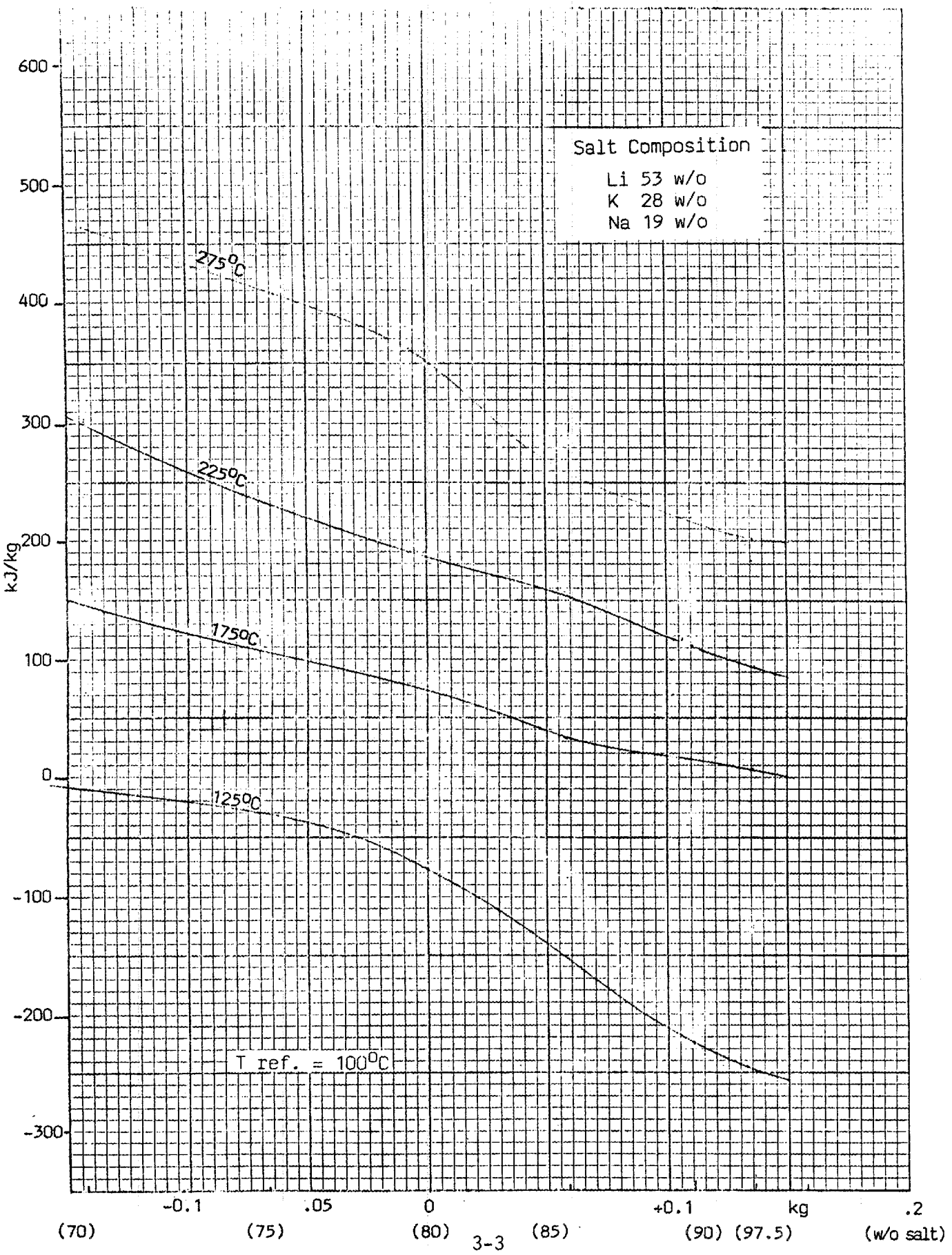

TABLE A3

VALUES USED IN CALCULATION OF MERKEL DIAGRAM

Conc.	t	t'	dt/dt'	P	ΔH'	v'	v	ΔH	H_v	H_v	$\bar{H}$	$\int_{t_0}^{t} H\,d\omega$	H_0	H	H
w/o	C	C		bar	kJ/kg	m³/kg	m³/kg	kJ/kg	kJ/kg	kJ/kg	kJ/kg	kJ/kg	kJ/kg	kJ/kg	kJ/kg
92.5	125	500	1.5405	.12344	2381.9	12037.	16202.0	2564.2	2734.4	2315.3	-248.9	-23.49	57.43	93.5	512.6
	175	82.46	1.5405	.5230	2301.95	3108.7	3969.4	2401.5	2828.2	2409.1	9.6	4.784	157.83	177.0	596.1
	225	114.91	1.5405	1.6853	2216.5	1039.9	1355.0	2406.7	2921.6	2502.5	95.8	22.54	238.97	250.2	669.3
	275	147.37	1.5405	4.4314	2122.2	420.1	560.06	2394.3	3013.7	2594.6	200.3	31.06	300.83	311.0	730.1
90	125	58.409	1.4348	.18545	2361.5	8228.7	10532.9	2529.9	2733.8	2314.7	-215.1	-17.86	57.43	84.7	508.8
	175	93.257	1.4348	.7926	2274.3	2106.3	2599.14	2392.4	2826.6	2407.5	15.1	4.510	157.83	172.5	591.6
	225	128.106	1.4348	2.55616	2179.5	705.4	892.54	2386.1	2918.0	2498.9	112.8	20.03	238.97	246.3	665.4
	275	162.954	1.4348	6.6550	2072.5	286.2	373.12	2367.1	3007.0	2587.9	220.8	30.57	300.83	304.0	723.1
85	125	68.88	1.3312	2.9699	2335.9	5280.4	6197.2	2397.3	2732.8	2313.7	-83.6	-6.645	57.43	68.0	487.1
	175	106.44	1.3312	1.2895	2238.5	1355.8	1607.8	2390.0	2823.9	2404.8	34.80	3.240	157.83	164.3	583.4
	225	144.00	1.3312	4.0398	2132.5	458.17	559.35	2335.5	2911.9	2492.8	157.3	13.03	238.97	240.1	659.2
	275	181.56	1.3312	10.3847	2009.0	185.73	236.55	2317.1	2995.4	2576.3	259.2	18.02	300.83	300.5	719.6
80	125	78.23	1.2632	.49089	2312.6	3647.3	4198.5	2388.4	2731.5	2312.4	-76.0	0	57.43	57.4	476.5
	175	119.81	1.2632	1.8591	2208.5	952.5	1105.9	2327.0	2820.5	2401.4	74.4	0	157.83	157.8	576.9
	225	157.90	1.2632	5.7791	2090.7	327.05	375.70	2199.8	2909.6	2485.5	285.7	0	238.97	239.0	658.1
	275	196.98	1.2632	14.5759	1951.9	135.40	166.09	2209.3	2981.9	2562.8	353.5	0	300.83	300.8	719.9
70	125	91.790	1.1795	.74888	2278.2	2221.2	2949.4	2319.3	2728.7	2309.6	-9.6	-4.82	57.43	54.5	473.6
	175	134.13	1.1795	3.0510	2162.0	576.41	669.48	2247.1	2813.2	2394.1	147.0	-15.82	157.83	151.9	571.0
	225	176.52	1.1795	9.2427	2026.8	209.56	238.61	2167.5	2889.2	2470.1	303.6	-34.14	238.97	239.0	658.1
	275	218.91	1.1795	22.699	1862.5	87.95	103.50	2070.1	2954.0	2534.9	464.8	-58.93	300.83	314.8	733.9

From Duhring diagram. From Steam Tables (Harr, 1984) $T_{ref.} = 100^{o}C$ $T_{ref.} = 0^{o}C$

INTERNAL DISTRIBUTION

1. M. R. Ally
2. J. Braunstein
3. R. S. Carlsmith
4. R. C. DeVault
5. W. Fulkerson
6-10. S. I. Kaplan
11. F. C. Maienschein, Consultant
12. M. A. Kuliasha
13. S. H. McConathy
14. M. R. Patterson
15. H. Perez-Blanco
16-17. Central Research Library
18. Document Reference Section
19. Laboratory Records - RC
20-21. Laboratory Records
22. ORNL Patent Section

EXTERNAL DISTRIBUTION

23. W. J. Biermann, 45 Foxcroft Drive, Fayetteville, NY 13066
24. J. M. Calm, Electric Power Research Institute, P. O. Box 10412, Palo Alto, CA 94303
25. Dr. J. G. Carbonell, Associate Professor of Computer Science, Carnegie-Mellon University, Pittsburgh, PA 15213
26. G. Douglas Carver, TVA, 703 Power Building, Chattanooga, TN 37402
27. R. N. Chappell, DOE Idaho Operations Office, 785 DOE Place, Idaho Falls, ID 83402
28. D. C. Erickson, Energy Concepts Company, 627 Ridgely Avenue, Annapolis, MD 21401
29. P. D. Fairchild, Electric Power Research Institute, 3412 Hillview Avenue, P. O. Box 10412, Palo Alto, CA 94303
30. R. J. Fiskum, CE-132, FORSTL, GF-217, Department of Energy, 1000 Independence Avenue, S.W., Washington, D.C. 20585
31. Joel Gilbert, Dames & Moore, Inc., 7101 Wisconsin Avenue, Suite 700, Bethesda, MD 20814
32. Dr. S. M. Gillis, Dean, Graduate School, Duke University, 4875 Duke Station, Durham, NC 27706
33. G. Grossman, Technion-Israel Institute of Technology, Faculty of Mechanical Engineering, Haifa, Israel
34. W. T. Hanna, Battelle Columbus Laboratories, 505 King Avenue, Columbus, OH 43201
35. F. C. Hayes, Trane Company, 3600 Pammel Creek Road, LaCrosse, WI 54601
36. Dr. F. R. Kalhammer, Vice President, Electric Power Research Institute, P. O. Box 10412, Palo Alto, CA 94303
37. Alan Karp, Electric Power Research Institute, Energy Management and Utilization Division, P. O. Box 10412, Palo Alto, CA 94303
38. Dr. R. E. Kasperson, Professor of Government and Geography, Graduate School of Geography, Clark University, Worcester, MA 01610
39. Dr. Martin Lessen, Consulting Engineer, 12 Country Club Drive, Rochester, NY 14618
40. R. A. Macriss, Institute of Gas Technology, 3424 South State Street, Chicago, IL 60616

41. L. A. McNeely, 7310 Steinmeier Drive, Indianapolis, IN 46250
42. D. K. Miller, Borg-Warner Air Conditioning, Inc., P. O. Box 1592, York, PA 17405
43. J. I. Mills, EG&G-Idaho, Inc., P. O. Box 1625-WCB, Idaho Falls, ID 83415
44. B. A. Phillips, Phillips Engineering Company, 721 Pleasant Street, St. Joseph, MI 49085
45. R. Radermacher, University of Maryland, Department of Mechanical Engineering, College Park, MD 20742
46. W. J. Rebello, PAR Enterprises, 11928 Appling Valley Road, Fairfax, VA 22030
47. R. C. Reimann, Carrier Corp., P. O. Box 4808, Syracuse, NY 13221
48. S. L. Richlen, U. S. Department of Energy, Office of Industrial Programs, CE-141 FORSTL, 1000 Independence Avenue SW, Washington, DC 20585
49. U. Rockenfeller, Rocky Research Company, 1453 Rawhide Road, Boulder City, NV 89005
50. J. D. Ryan, CE-132, FORSTL, GF-217, Department of Energy, 1000 Independence Avenue, S.W., Washington, D.C., 20585
51. D. S. Severson, Gas Research Institute, 8800 West Bryn Mawr Avenue, Chicago, IL 60631
52. Professor Sam V. Shelton, Georgia Institute of Technology, Department of Mechanical Engineering, Atlanta, GA 30332
53. J. J. Tuzson, Gas Research Institute, 8800 West Bryn Mawr Avenue, Chicago, IL 60631

54-63. Energy Conservation Distribution, Oak Ridge National Laboratory, Bldg. 9102-2, Room 103, Oak Ridge, TN 37831

64. Office of the Assistant Manager for Energy Research and Development, U. S. Department of Energy, Oak Ridge Operations, Oak Ridge, TN 37831

65-91. Technical Information Center, U. S. Department of Energy, P. O. Box 62, Oak Ridge, TN 37831